JCM
Journals.ASM.org

Identification of TL-Om1, an Adult T-Cell Leukemia (ATL) Cell Line, as Reference Material for Quantitative PCR for Human T-Lymphotropic Virus 1

Madoka Kuramitsu,[a] Kazu Okuma,[a] Makoto Yamagishi,[b] Tadanori Yamochi,[b] Sanaz Firouzi,[b] Haruka Momose,[a] Takuo Mizukami,[a] Kazuya Takizawa,[a] Kumiko Araki,[a] Kazuo Sugamura,[c] Kazunari Yamaguchi,[a] Toshiki Watanabe,[b] Isao Hamaguchi[a]

Department of Safety Research on Blood and Biological Products, National Institute of Infectious Diseases, Tokyo, Japan[a]; Department of Medical Genome Sciences, Laboratory of Tumor Cell Biology, Graduate School of Frontier Sciences, The University of Tokyo, Tokyo, Japan[b]; Division of Molecular and Cellular Oncology, Miyagi Cancer Center Research Institute, Natori, Japan[c]

Quantitative PCR (qPCR) for human T-lymphotropic virus 1 (HTLV-1) is useful for measuring the amount of integrated HTLV-1 proviral DNA in peripheral blood mononuclear cells. Many laboratories in Japan have developed different HTLV-1 qPCR methods. However, when six independent laboratories analyzed the proviral load of the same samples, there was a 5-fold difference in their results. To standardize HTLV-1 qPCR, preparation of a well-defined reference material is needed. We analyzed the integrated HTLV-1 genome and the internal control (IC) genes of TL-Om1, a cell line derived from adult T-cell leukemia, to confirm its suitability as a reference material for HTLV-1 qPCR. Fluorescent *in situ* hybridization (FISH) showed that HTLV-1 provirus was monoclonally integrated in chromosome 1 at the site of 1p13 in the TL-Om1 genome. HTLV-1 proviral genome was not transferred from TL-Om1 to an uninfected T-cell line, suggesting that the HTLV-1 proviral copy number in TL-Om1 cells is stable. To determine the copy number of HTLV-1 provirus and IC genes in TL-Om1 cells, we used FISH, digital PCR, and qPCR. HTLV-1 copy numbers obtained by these three methods were similar, suggesting that their results were accurate. Also, the ratio of the copy number of HTLV-1 provirus to one of the IC genes, RNase P, was consistent for all three methods. These findings indicate that TL-Om1 cells are an appropriate reference material for HTLV-1 qPCR.

Human T-lymphotropic virus 1 (HTLV-1) was the first retrovirus to be found in humans (1, 2). HTLV-1 is a cause of adult T-cell leukemia (ATL), HTLV-1-associated myelopathy/tropical spastic paraparesis (HAM/TSP), and HTLV-1-associated uveitis (3). Areas where HTLV-1 is endemic are distributed across several different regions, including southern Japan, the Caribbean, South America, and tropical Africa (4, 5). A recent report has shown that the area affected by this infection has expanded from the southern part of Japan to the entire country, particularly the Tokyo metropolitan area (6). Diagnostic tests for HTLV-1 infection are performed mainly with serological assays, such as enzyme-linked immunoabsorbent assay, particle agglutination assay, and Western blotting. Recently, another diagnostic test has been developed. Quantitation of integrated proviral DNA in peripheral blood (proviral load [PVL]) can be performed by quantitative PCR (qPCR) as a risk assessment for ATL or HAM/TSP (7, 8).

A few studies reported that several samples were positive for viral DNA when tested by PCR even though those samples had been found seroindeterminate for HTLV-1 when tested by Western blotting (9, 10). Their results suggest that HTLV-1 qPCR could be used as an additional test to confirm infection in seroindeterminate samples.

Although many laboratories have developed qPCR methods for HTLV-1 detection in Japan, a wide variety of testing methods are used. For example, the target region, primers and probes, and internal control (IC) genes vary among the laboratories (8, 11–15). These variations lead to significant differences in HTLV-1 PVL when these laboratories measure the same samples (16). As a consequence of these differences, comparison of quantitative data between laboratories will continue to be difficult without standardization.

One possible solution is to establish a reference material, which is indispensable for standardizing multicenter test results. The target material for HTLV-1 qPCR is genomic DNA (gDNA) from peripheral blood mononuclear cells (PBMCs). Therefore, HTLV-1-infected cells would be an ideal source for a reference material. To date, many cell lines from ATL patients have been established, but few of them have been well characterized for the genomic features associated with reference materials for HTLV-1 qPCR.

In this study, we investigated the genomic structure of one of these ATL cell lines, TL-Om1, to establish it as a reference material for HTLV-1 nucleic acid amplification techniques (NATs), namely, HTLV-1 clonality, karyotyping, proviral sequencing, integration sites, and determination of gene copy number of HTLV-1 and cellular genes for IC.

Received 5 August 2014 Returned for modification 23 September 2014
Accepted 5 December 2014
Accepted manuscript posted online 10 December 2014
Citation Kuramitsu M, Okuma K, Yamagishi M, Yamochi T, Firouzi S, Momose H, Mizukami T, Takizawa K, Araki K, Sugamura K, Yamaguchi K, Watanabe T, Hamaguchi I. 2015. Identification of TL-Om1, an adult T-cell leukemia (ATL) cell line, as reference material for quantitative PCR for human T-lymphotropic virus 1. J Clin Microbiol 53:587–596. doi:10.1128/JCM.02254-14.
Editor: A. M. Caliendo
Address correspondence to Isao Hamaguchi, 130hama@niid.go.jp.
Supplemental material for this article may be found at http://dx.doi.org/10.1128/JCM.02254-14.

doi:10.1128/JCM.02254-14

TABLE 1 Primers used for qPCR of HTLV-1 and IC genes

Target gene	Forward name	Forward sequence	Reverse name	Reverse sequence	Size (bp)	Primer correction factor	
						Plasmid	gDNA
HTLV-1 gene	LTR202F	ACAATGACCATGAGCCCCAAA	LTR202R	TTAGTCTGGGCCCTGACCT	101	0.9869	
	LTR215F	GCTCGCATCTCTCCTTCAC	LTR215R	AGTTCAGGAGGCACCACA	102	0.9942	
	LTR005F	CCTGACCCTGCTTGCTCAAC	LTR005R	TCAGTCGTGAATGAAAGGGAAAG	99	0.9917	
	056F	TAGTCCCACCCTGTTCGAAATG	056R	GCCAGGAGAATGTCATCCATGT	105	1.0013	
	084F	CCTGCCCCGCTTACTATCG	084R	GGCATCTGTGAGAGCGTTGA	102	0.9922	
	153F	TTGTCGCGCTACTCCTTCTTG	153R	AGGGATGACTCAGGGTTTATAAGAGA	118	0.9792	
	pX2-S[a]	CGGATACCCAGTCTACGTGTT	pX2-AS[a]	CAGTAGGGCGTGACGATGTA	100	0.9944	
RNaseP (RPPH1) gene	RPPH1-05F	TATGCACAATTATGTAATCCCCAAA	RPPH1-05R	CCAGCTCCCTATAACCTGCACTT	100	1.0025	1.0012
	RPPH1-08F	GCCGGAGCTTGGAACAGA	RPPH1-08R	AATGGGCGGAGGAGAGTAGTCT	109	0.9956	0.9937
	RPPH1-12F	AGGAAGCCCACGAAAATTCTAATT	RPPH1-12R	GTCCCCATACTCGGTGATTCTC	101	1.0019	1.0052
Albumin (ALB) gene	ALB-07F	TGCAATGAACACAGGAGAGCTACTA	ALB-07R	CCACCCAGGTAACAAAATTAGCAT	103	0.9971	0.9964
	ALB-19F	CCTGATGCTTCTCAGCCTGTT	ALB-19R	TCCATTTAAGAGTGTGTGTGGTAGGT	100	1.0019	1.0045
	ALB-26F	TGCATTGCCGAAGTGGAAA	ALB-26R	CCTCAGCATAGTTTTTGCAAACA	100	1.0038	1.0078
β-Actin (ACTB) gene	ACTB-06F	TCTGGTGTTTGTCTCTCTGACTAGGT	ACTB-06R	CCGCTTTACACCAGCCTCAT	100		0.9965
	ACTB-12F	TCCTGGGTGAGTGGAGACTGT	ACTB-12R	CCATGCCTGAGAGGGAAATG	107		1.0016
	ACTB-21F	AGCATCCCCCAAAGTTCACA	ACTB-21R	GGACTTCCTGTAACAACGCATCT	101		1.0106
CD81 gene	CD81-01F	GACACATCCCAAGGGTGCTT	CD81-01R	GGACTCAGTTCTCAATGCTTTGC	107		1.0015
	CD81-10F	ACCACGCCTTGCCCTTCT	CD81-10R	GAATCACGCCACTTCCATAACTG	111		1.0021
	CD81-21F	GGTGCACACAGCATGCATTT	CD81-21R	GTGCGCCTCTGGGTAATCAT	102		1.0009
β-Globin (HBB) gene	HBB-11F	TTGGACCCAGAGGTTCTTTGAG	HBB-11R	GGCACCGAGCACTTTCTTG	103		1.0021
	HBB-15F	AGCAGCTACAATCCAGCTACCAT	HBB-15R	GAGGTATGAACATGATTAGCAAAAGG	105		1.0033
	HBB-24F	CCCACCCCAAATGGAAGTC	HBB-24R	AGCACCATAAGGGACATGATAAGG	104		1.0111
RAG-1 gene	RAG1-03F	GCAATCCCATTTGTCCACTTTT	RAG1-03R	TCCCACTGGCCTGCATTACTA	100		1.0045
	RAG1-27F	GAAGTTTAGCAGTGCCCCATGT	RAG1-27R	ACGGGCAGTGTTGCAGATG	100		1.0006
	RAG1-32F	TCAAAGTCATGGGCAGCTATTGT	RAG1-32R	AGGGAATTCAAGACGCTCAGAA	100		0.9993

[a] Primer sequences were previously reported in reference 11.

MATERIALS AND METHODS

Cells and gDNA preparation. Jurkat clone E6-1 cells were obtained from the American Type Culture Collection. HUT102 and SLB-1 cells, which are HTLV-1-infected cell lines, were a kind gift from Masahiro Fujii (Division of Virology, Niigata University Graduate School of Medical and Dental Sciences). PBMCs were kindly provided by the Japanese Red Cross or purchased from AllCells (Alameda, CA, USA). TL-Om1 cells, an ATL-derived cell line established by Sugamura et al. (17), were maintained in RPMI 1640 (Sigma, St. Louis, MO, USA) containing 10% fetal bovine serum (FBS) supplemented with 100 U/ml penicillin-streptomycin (Invitrogen, Carlsbad, CA, USA), 2 mmol/liter L-glutamine, and 10 ng/ml interleukin-2 (PeproTech, London, United Kingdom). Jurkat, HUT102, and SLB-1 cells were maintained in RPMI 1640 containing 10% FBS supplemented with 100 U/ml penicillin-streptomycin and 2 mmol/liter L-glutamine. DNA was extracted using a QIAamp DNA blood mini or maxi kit (Qiagen, Valencia, CA, USA).

Southern blotting. Southern blotting was performed by SRL Inc. (Tokyo, Japan). DNA was digested with EcoRI and PstI and separated on a 0.8% agarose gel as previously reported (18, 19). DNA was transferred onto nylon membranes (Roche, Mannheim, Germany). The membrane was hybridized with digoxigenin (DIG)-labeled HTLV-1 probe at 42°C overnight. DNA fragments for HTLV-1 probes were obtained from Oncor Inc. (Gaithersburg, MD, USA). Sense and antisense HTLV-1 DNA probes were prepared by random primed labeling using a DIG-High Prime kit (Roche). After the membrane was washed, HTLV-1 probe signals were obtained using a DIG luminescent detection kit (Roche).

FISH analysis. To stop the cell cycle at M phase, Colcemid (Sigma) was added to the cell culture medium at a concentration of 0.02 μg/ml and incubated for 1 h. Cells were harvested and washed with phosphate-buffered saline (PBS). After treatment with 0.075 M KCl hypotonic solution at 37°C for 1 h, cells were fixed with a solution containing acetic acid and methanol (3:1). Cells were fixed to a glass slide and dried. The complete HTLV-1 genome inserted in pUC18 (15) was used as a probe for provirus, bacterial artificial chromosome (BAC) clone RP11-919G18 was used as a probe for the albumin (ALB) gene, and BAC clones CTD-2326H15 and RP11-203M5 were used as probes for the RNase P (RPPH1) gene. BAC clones were selected from NCBI (http://www.ncbi.nlm.nih.gov/clone/) and were purchased from Advanced Geno Techs Co. (Tsukuba, Japan). The probe for 1q44 was commercially prepared by Chromosome Science Labo Inc. (Sapporo, Japan). For the detection of ALB and RPPH1 genes, the BAC clones were labeled with cyanine 3 (Cy3) and Cy5, respectively. For the detection of provirus, the DIG-labeled probe was prepared by the nick translation method. The probe was hybridized to the sample at 70°C for 5 min, followed by incubation at 37°C overnight. The probe was stained with anti-DIG-Cy3 antibody. Signals were detected by a Leica DMRA2 system and analyzed with Leica CW4000 fluorescent *in situ* hybridization (FISH) software (Wetzlar, Germany).

Splinkerette PCR analysis. Splinkerette PCR was performed as previously reported (20). The first-round PCR was performed as indicated in reference 20. The second-round, nested PCR was performed using the HTLV-1 long-terminal-repeat (LTR)-specific primer. The nested PCR product was loaded onto 3% Tris-acetate-EDTA buffer (TAE) agarose gels. Two distinct DNA bands were cut from the agarose gel and purified using a QIAquick gel extraction kit (Qiagen). After thymine and adenine (TA) cloning, each band was sequenced by the Sanger method (21).

Inverse PCR analysis. TL-Om1 gDNA was digested with BamHI or XbaI. Digested DNA was purified by phenol-chloroform extraction followed by ethanol precipitation. Briefly, 1/10 volume of 3 M sodium acetate and 2.5 volume of 100% ethanol were added to the sample. After centrifugation at $2 \times 10^4 \times g$ for 15 min, the DNA pellet was washed with 70% ethanol and then air dried. Purified DNA was self-ligated using a Ligation-Convenience kit (Nippon Gene, Tokyo, Japan). Ligated DNA was purified again by phenol-chloroform extraction followed by ethanol precipitation. PCR was performed with KOD FX (Toyobo, Osaka, Japan). The PCR mixture contained 20 ng gDNA, 0.4 mM forward and reverse primers, 1 mM deoxynucleoside triphosphate (dNTP), 1× KOD FX buffer, and 0.5 U KOD FX in a total volume of 25 μl, in duplicate. The forward primer sequence was 5′-ACAAATACACCTTGCAATCCTATG G-3′, and the reverse primer sequence was 5′-CGCTTGGGAGACTTCT TGCT-3′. PCR mixtures were denatured at 94°C for 2 min, followed by 34 cycles of 98°C for 10 s and 68°C for 10 min. PCR products were loaded onto 0.8% agarose gels and detected by LAS-3000 (Fujifilm, Tokyo, Japan).

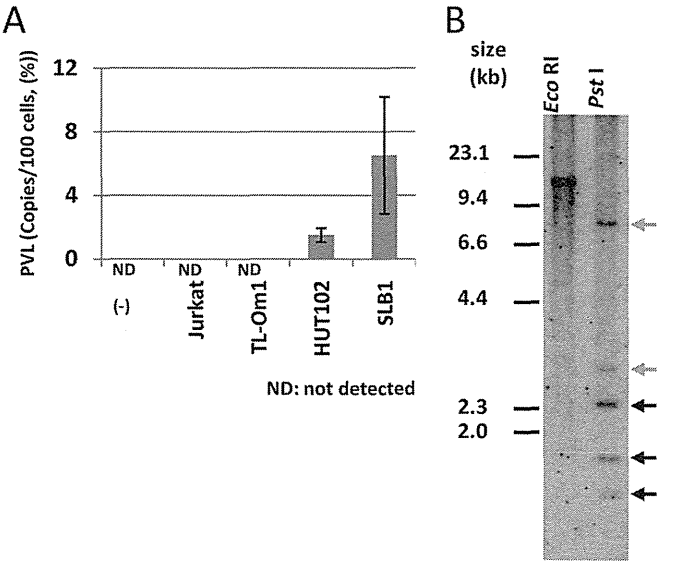

FIG 1 Infectivity and clonality of HTLV-1 provirus in TL-Om1 cells. (A) Mitomycin C-treated Jurkat, TL-Om1, HUT102, and SLB1 cells were cocultured with Jurkat cells. PVL (%) was measured 2 weeks later by qPCR. (B) gDNA from TL-Om1 cells digested with EcoRI or PstI was subjected to Southern blotting probed by the full HTLV-1 genome. Three black arrows show bands for typical HTLV-1 genomic sequences; two gray arrows show bands for host genomic sequences ligated to the HTLV-1 genome. Because the EcoRI site is not included in the HTLV-1 sequence, the number of bands indicates the number of clones in the cells. Detection of two gray bands indicates that there is a pair of 5′ and 3′ HTLV-1 genomes conjugated with the host genome, signifying that the HTLV-1 provirus is monoclonal. On the other hand, detection of more than two gray bands indicates that it is multiclonal.

Genomic long PCR. Genomic long PCRs were performed using KOD FX (Toyobo). Primers are listed in Table S1 in the supplemental material. The conditions for the PCR mixture and thermal cycling program were the same as those for the inverse PCR analysis.

DNA sequencing analysis. The genomic long PCR and inverse PCR products were purified by a GenElute PCR Clean Up kit (Sigma). Direct sequencing was performed using a BigDye Terminator v3.1 sequencing kit (Applied Biosystems, Foster City, CA, USA). Sequence primers are listed in Table S2 in the supplemental material. Sequences were read and analyzed using a 3120× genetic analyzer (Applied Biosystems).

Synchronized qPCR analysis. The primers used for the synchronized qPCR amplification are listed in Table 1. The PCR mixture was prepared with SYBR premix *Ex Taq* II (TaKaRa, Tokyo, Japan) containing 100 ng gDNA and 0.4 mM forward and reverse primers in a total volume of 15 μl, in triplicate. PCR was performed according to the manufacturer's protocol. The ΔC_T(RPPH1) value (where C_T is threshold cycle) was calculated by the following equation: ΔC_T(RPPH1) = average C_T of target gene primer results − average C_T of RPPH1. The gene copy number was calculated by the following equation: target gene copy number (N) = copy number determined by FISH $\times 2^{-\Delta CT(\mathrm{RPPH1})}$. Using normal PBMCs or plasmids, the primer correction factor, which can compensate for small differences in amplification efficiency among different primers, was calculated. The correction factor was determined by the difference of each C_T

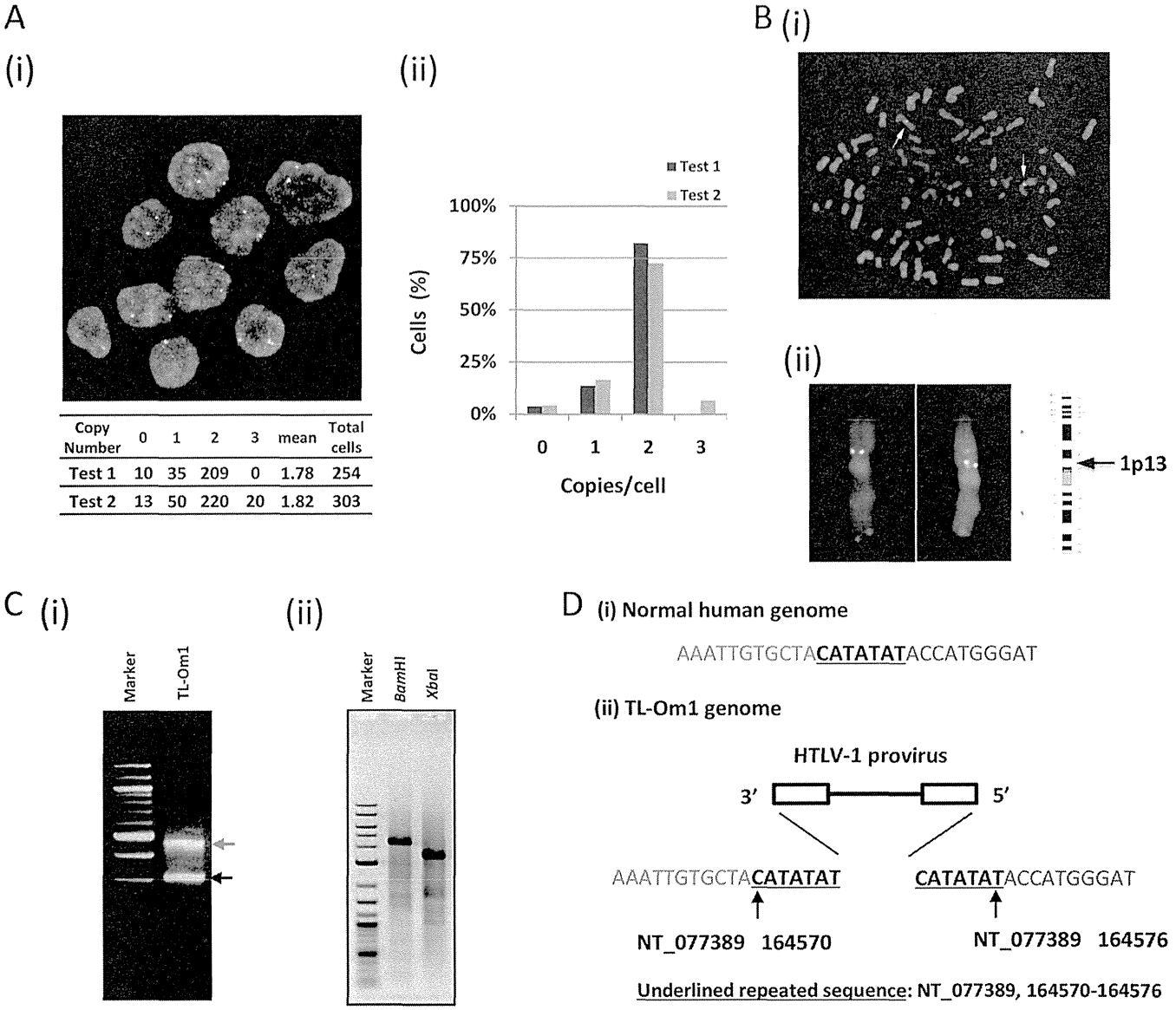

Copy Number	0	1	2	3	mean	Total cells
Test 1	10	35	209	0	1.78	254
Test 2	13	50	220	20	1.82	303

FIG 2 Clonality, copy number, and integration site of HTLV-1 in TL-Om1 cells. (A) HTLV-1 proviral copy number per cell was determined by FISH using an HTLV-1 full-genome probe. (i) Yellow signals indicate the HTLV-1 probe. Lower table shows the counts of HTLV-1 signals per cell. (ii) Vertical axis indicates percentage counts of each fraction in relation to total cells. Data were the results from two independent analyses. (B) Number of HTLV-1 integrated chromosomes was determined in metaphase cells with the HTLV-1 and 1q44 probes. (i, ii) Yellow signals indicate the HTLV-1 probe, and red signals indicate the 1q44 probe. All HTLV-1 signals were located on chromosome 1. HTLV-1 signals on chromosome 1 were positioned at 1p13. (C) Determination of the HTLV-1 integration site in TL-Om1 cells. (i) The 3′ integration site was determined by Splinkerette PCR with an HTLV-1-specific primer. PCR products were subjected to agarose gel electrophoresis. (ii) BamHI- or XbaI-digested TL-Om1 genomes were self-ligated and subjected to inverse PCR with an HTLV-1-specific primer set. PCR products were subjected to agarose gel electrophoresis. (D) 5′ and 3′ HTLV-1 integration sites were determined by a sequencing analysis of DNA fragments from both Splinkerette and inverse PCR. (i) Normal human sequence; (ii) determined HTLV-1 integration site. HTLV-1 was inversely integrated at chromosome 1: NT_077389, 164570 to 164576.

value of target gene primers from the average C_T value of RPPH1 primers (Table 1). The correction value was calculated as follows: correction C_T value = correction factor × actual C_T value. By applying the correction factors, we reduced the limits of error of the C_T values to 0.1 cycles with normal PBMCs (data not shown).

Digital PCR analysis. Primers and probes for digital PCR analysis of HTLV-1 were previously reported (11, 15). In brief, the primers and probe for HTLV-1 were as follows: forward, 5′-CGGATACCCAGTCTACGTG TT-3′; reverse, 5′-CAGTAGGGCGTGACGATGTA-3′; probe, FAM-5′-CTGTGTACAAGGCGACTGGTGCC-3′-TAMRA (where FAM is 6-carboxyfluorescein and TAMRA is 6-carboxytetramethylrhodamine). The primers and probe for albumin were as follows: forward, 5′-TGTCAT CTCTTGTGGGCTGT-3′; reverse, 5′-GGTTCTCTTTCACTGACATC TGC-3′; probe, FAM-5′-CCTGTCATGCCCACACAAATCTCTCC-3′-TAMRA. The mixture of primers and probe for RPPH1 was purchased from Applied Biosystems. The PCR mixture was prepared using 2× digital droplet PCR (ddPCR) supermix for probes (Bio-Rad, Hercules, CA, USA). Droplets were prepared on a QX100 droplet generator (Bio-Rad). PCR was performed with a LifePro thermal cycler (Bio-Rad) and detected with a QX100 droplet reader (Bio-Rad). Data were means of triplicate analysis.

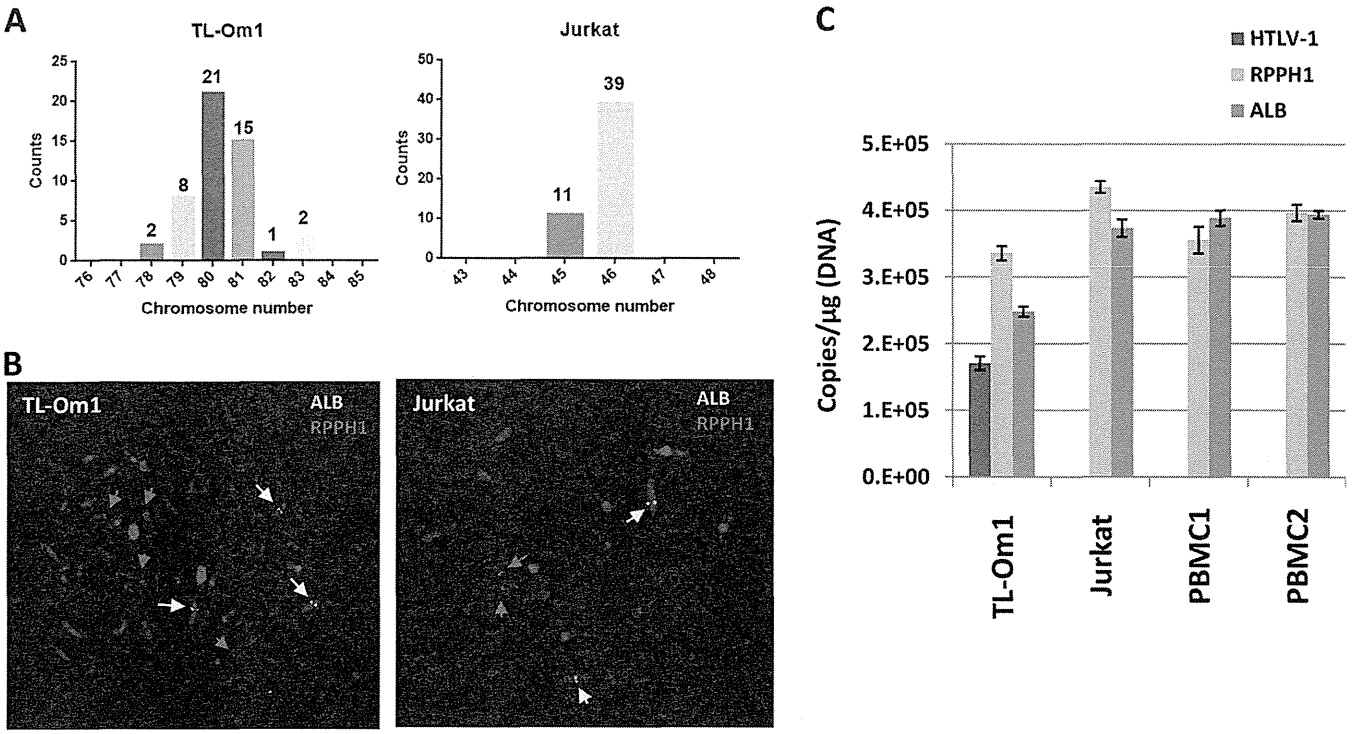

FIG 3 Gene copy number of IC cellular genes for HTLV-1 qPCR. (A) The number of chromosomes in TL-Om1 and Jurkat cells at metaphase was counted. Horizontal line indicates the number of chromosomes per cell. (B) Representative FISH images of TL-Om1 and Jurkat cells at metaphase. Yellow and red arrows indicate signals for ALB and RPPH1 probes, respectively. Left panel shows three signals for ALB and four for RPPH1; right panel shows two signals for ALB and two for RPPH1. (C) Determination of the gene copy number of HTLV-1, RPPH1, and ALB genes by digital PCR. gDNA of TL-Om1 and Jurkat cells and of PBMCs from two healthy donors were subjected to digital PCR. Data show the absolute copy number of HTLV-1, RPPH1, and ALB genes per microgram of gDNA. Bars are means from triplicate analyses.

***In vitro* HTLV-1 infectivity test.** Frozen cells were thawed and immediately cultured for a week. Exponentially growing cells were used for the assay. Jurkat, TL-Om1, SLB1, and HUT102 cells were treated with 50 μg/ml mitomycin C (Kyowa Hakko Kirin, Tokyo, Japan) and incubated for 1 h at 37°C. After being washed twice with 2% FBS-PBS, 1×10^5 cells were added to culture medium containing 1×10^6 Jurkat cells. Mitomycin C was used to block the growth of ATL cell lines added to Jurkat cells. Cells were cocultured for 2 weeks and then subjected to qPCR to determine PVL, as described previously (11).

RESULTS

HTLV-1 infectivity in TL-Om1 cells. We investigated the production potential of infective virus to ascertain the clonal stability of HTLV-1 integration *in vitro*. Mitomycin C-treated TL-Om1 cells were cocultured with Jurkat cells for 2 weeks. At the end of the 2 weeks, no HTLV-1 integration was observed in the Jurkat cells that were cocultured with TL-Om1 cells, while HTLV-1 integration was observed when Jurkat cells were similarly cocultured with SLB-1 and HUT102 cells (Fig. 1A). These findings suggested that the production of infective HTLV-1 particles from TL-Om1 cells was low or diminished; thus, the increase in copy number over the course of cell culture was thought to be negligible. If TL-Om1 cells had infectious potential, the clonality of HTLV-1 provirus in them would vary because of the mutual HTLV-1 infections between cells. To evaluate the clonality of HTLV-1 provirus in TL-Om1 cells, TL-Om1 gDNA was analyzed by Southern blotting. EcoRI-digested gDNA showed a single band, while PstI digestion produced five DNA bands that contained an HTLV-1 sequence (Fig. 1B). Three of the five DNA bands were HTVL-1 internal sequences. The other two DNA bands contained either 5′ or 3′ HTLV-1 sequences ligated with the host genome (Fig. 1B). These fragment patterns indicated that HTLV-1 provirus integration in TL-Om1 cells was monoclonal.

Determination of copy number and integration site of HTLV-1 provirus by FISH. To confirm the clonality and copy number of HTLV-1 provirus and of IC genes in detail, we performed a FISH analysis. There were one or two signals of HTLV-1 provirus in the cells. The mean proviral copy number was calculated at 1.8 copies/cell from the count of signals with >250 cells in two independent analyses (Fig. 2Ai and ii). Double-staining of the TL-Om1 genome with both HTLV-1 and 1q44 probes in meta-

TABLE 2 Gene copy number of IC genes determined by FISH

Karyotype	Gene copy no.			
	TL-Om1 (20 analyzed cells)		Jurkat (20 analyzed cells)	
	RPPH1 gene	ALB gene	RPPH1 gene	ALB gene
2N	0	0	20	20
3N	1	20	0	0
4N	19	0	0	0
Average	3.95	3	2	2
Ratio to the RPPH1 gene	1	0.76	1	1

TABLE 3 Summary of ratio of gene copy numbers to the RPPH1 gene

Method	Cell line	Gene copy no. ratio to the RPPH1 gene							
		RPPH1 gene	ALB gene	ACTB gene	CD81 gene	HBB gene	RAG-1 gene	HTLV-1 gene	LTR gene
FISH	TL-Om1	1.00	0.76					0.46	
	Jurkat	1.00	1.00						
Digital PCR	TL-Om1	1.00	0.74					0.51	
	Jurkat	1.00	0.86						
	PBMC1	1.00	1.09						
	PBMC2	1.00	0.99						
qPCR (plasmid)	TL-Om1	1.00	0.74					0.48	1.02
	Jurkat	1.00	0.92						
qPCR (gDNA)	TL-Om1	1.00	0.74	1.18	0.99	0.92	0.94		
	Jurkat	1.00	0.95	1.07	0.99	0.90	1.08		
	PBMC 1	1.00	0.99	1.00	0.98	0.99	1.00		
	PBMC 2	1.00	1.01	1.01	0.99	1.00	1.01		

phase showed that all HTLV-1 DNA signals were located on chromosome 1 (Fig. 2Bi). When the number of copies of chromosome 1 was 1, 2, 3, or 4 per cell, the number of HTLV-1 proviruses per cell was 1, 1, 2, and 2, respectively (data not shown). HTLV-1 signals on chromosome 1 were positioned on the band of 1p13 (Fig. 2Bii). These results correlated well with the Southern blotting results that showed monoclonal integration.

Confirmation of integration site of HTLV-1 in TL-Om1 cells. To identify the integration site of monoclonal HTLV-1 provirus, Splinkerette PCR was performed with TL-Om1 gDNA. Two specific PCR products were obtained by gel electrophoresis (Fig. 2Ci). The DNA fragments were analyzed by direct sequencing. Sequencing analysis of the lower-molecular-weight DNA fragments (Fig. 2Ci, lower band) showed that they were provirus genomic sequences. Sequencing analysis of the higher-molecular-weight band showed that it contained host gDNA ligated to the 3′ LTR of HTLV-1. We also performed inverse PCR with TL-Om1 gDNA that was digested with BamHI or XbaI followed by self-ligation. Single DNA bands were obtained from both BamHI and XbaI self-ligated templates (Fig. 2Cii). Sequencing analysis demonstrated that both bands contained the same sequences. A BLAST search revealed that the sequence was located on chromosome 1. The integration site was identified, and the HTLV-1 provirus was integrated inversely in between the CATATAT repetitive sequences at the region of NT_077389 from nucleotides (nt) 164570 to 164576 on chromosome 1 (Fig. 2Di and ii).

We determined the full-length sequence of HTLV-1 provirus in TL-Om1 cells by genomic long PCR followed by direct sequencing. The length of HTLV-1 provirus was determined to be 8,941 bp (GenBank accession no. AB979451; see also Text S1 in the supplemental material). The percent identity to the HTLV-1 genomic sequence of the ATK-1 strain (accession no. J02029) was 98.7%. Compared with the full-length HTLV-1 genomic sequence of ATK-1, there was a 93-nt deletion in the *env* gene. The region that was deleted was equivalent to nt 5547 to 5669 of ATK-1. The deduced amino acid sequence of the deletion was 31 in-frame amino acids (Δ125–155 of Env). The deleted region was located on the receptor binding domain of Env (see Fig. S1 in the supplemental material).

Calculation of chromosome and gene copy numbers of HTLV-1, RPPH1, and ALB genes in TL-Om1 and Jurkat cells. We counted the chromosome number in TL-Om1 and Jurkat cells by FISH analysis. Jurkat cells were analyzed as one of the control cell lines. The chromosome number differed from 78 to 83 in TL-Om1 cells (Fig. 3A). The mean chromosome number was estimated at 80.2, which indicated that the karyotype of TL-Om1 cells was about 4*N*. There were 45 or 46 chromosomes in Jurkat cells, indicating that their karyotype is near that of normal human diploid cells (Fig. 3A and B and Table 2).

The absolute gene copy number of HTLV-1 provirus and IC genes was measured using digital PCR. gDNA from TL-Om1 cells, Jurkat cells, and PBMCs from two healthy donors was subjected to digital PCR and used to calculate the copy numbers of these genes (Fig. 3C). Although the ALB-to-RPPH1 gene copy number ratios in the two PBMC samples were 1.09 and 0.99, the ALB-to-RPPH1 gene copy number ratio in TL-Om1 cells was low (ratio of 0.74) (Table 3). The provirus-to-RPPH1 gene copy number ratio in TL-Om1 cells was 0.51 (Table 3). These results were consistent with the provirus- and ALB-to-RPPH1 gene copy number ratios estimated by FISH, which were 0.46 and 0.76, respectively (Table 3). The usefulness of TL-Om1 as a reference standard is strongly supported by the consistent results from the FISH and digital PCR analyses (Table 4).

Estimation of the gene copy number of HTLV-1 and IC genes by synchronized qPCR. We previously developed a method to determine inherited allelic deletions by using qPCR with primer sets that can amplify fragments synchronously, even though the

TABLE 4 Absolute gene copy number per microgram gDNA determined by digital PCR

Cell line	Gene copy no./μg gDNA[a]		
	HTLV-1 gene	RPPH1 gene	ALB gene
TL-Om1	170,171.1	335,452.3	248,410.8
Jurkat	NT	434,529.6	373,423.9
PBMC1	NT	355,116.1	388,650.0
PBMC2	NT	397,260.3	394,520.5

[a] Data are means of triplicate analysis. NT, not tested.

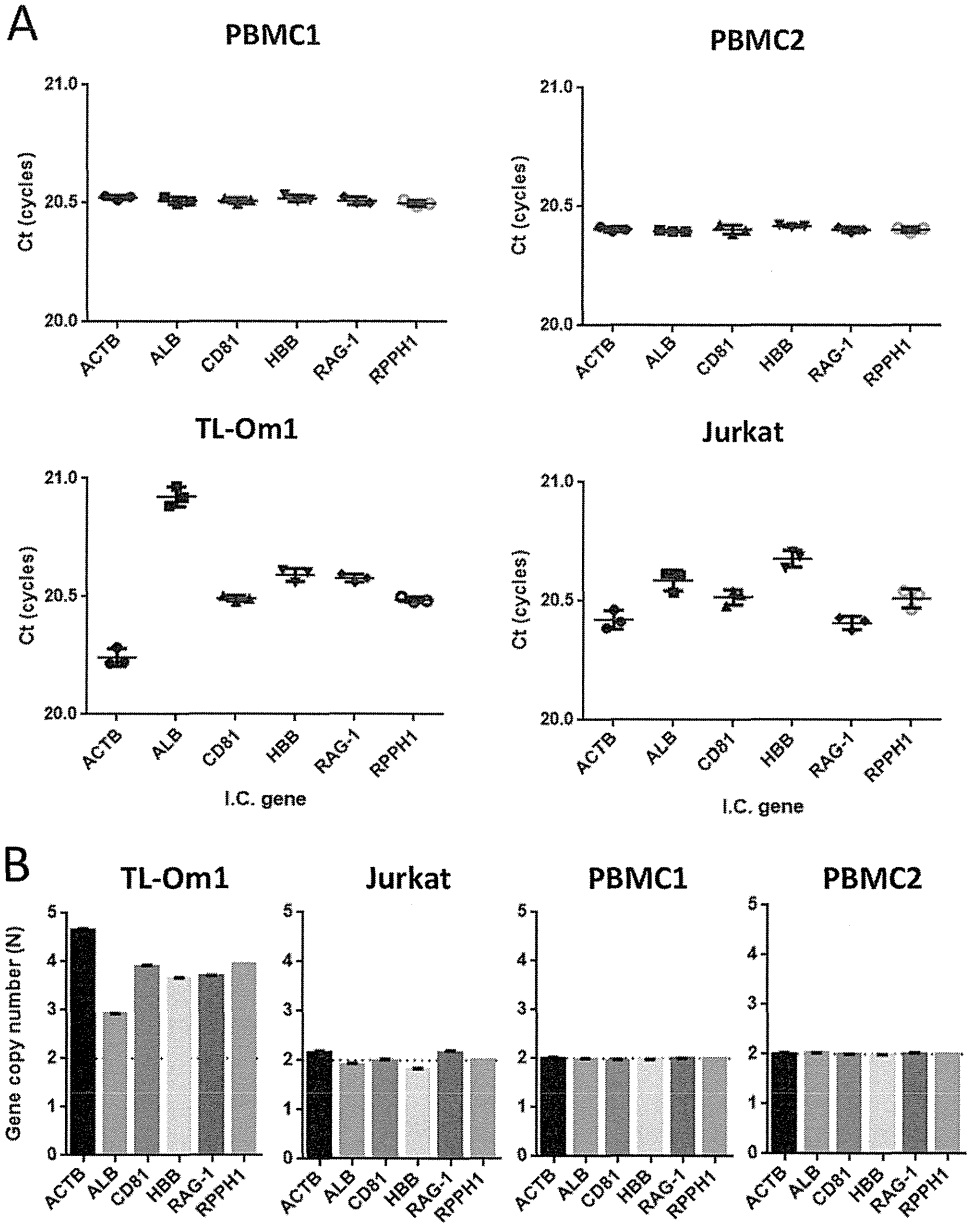

FIG 4 Estimation of gene copy number of IC genes in TL-Om1 cells by qPCR. gDNA of TL-Om1 and Jurkat cells and of PBMCs from two healthy donors was tested by qPCR with synchronous amplification primer sets for IC genes. (A) C_T scores (cycles) of each primer set for IC genes. Each dot indicates the mean from triplicate analyses. The C_T scores in the graph were the results of correction by the factors described in Table 1. (B) Estimated gene copy number of IC genes calculated using the difference in C_T scores from RPPH1. The copy numbers of IC genes of TL-Om1 and Jurkat cells were calculated based on FISH analysis for the RPPH1 gene. RPPH1 gene copy number from PBMCs was set as 2*N*. Equation for the estimation of gene copy number was as follows: gene copy number (N) = RPPH1 gene copy number determined by FISH analysis $\times 2^{-\Delta CT}$, $\Delta C_T = C_T$(target gene) $- C_T$(RPPH1).

target genes are different. The method shows that the difference in C_T value determines the difference in gene copy number. We used primer sets for HTLV-1 genes (LTR and coding regions) and ACTB, ALB, CD81, HBB, and RAG-1 IC genes (Table 1). To increase the specificity, we used primer correction factors, which compensate for the slight difference in PCR amplification efficiency between different primers for target genes. As shown in Fig. 4A, TL-Om1 and Jurkat cells did not show the complete synchronized amplifications that were observed in normal PBMCs. By setting the PCR amplification efficiency of all primer sets per cycle to approximately 2-fold, the ratio of the gene copy number against the RPPH1 gene was estimated using the difference in the mean C_T scores of the IC gene primer sets from the mean of those for the RPPH1 gene. The ratios of the gene copy number of the ALB gene to that of the RPPH1 gene in TL-Om1 and Jurkat cells were 0.74 and 0.92, respectively (Table 3). When the copy number of the RPPH1 gene in TL-Om1 cells was set at 3.95, which was determined by FISH analysis, the copy number of the IC genes was at least 2.9 (ALB gene) and at most 4.7 (ACTB gene) (Fig. 4B and Table 3).

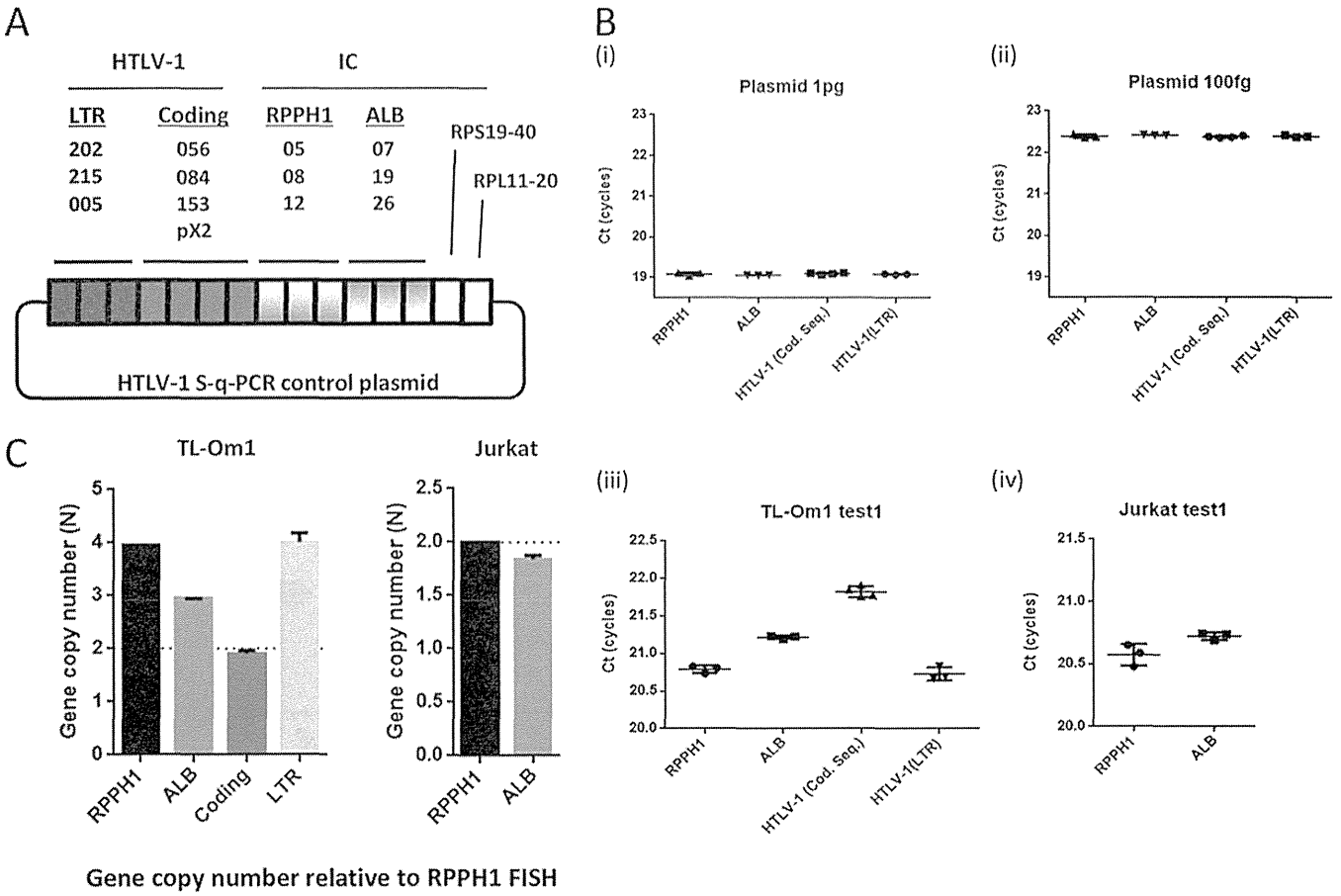

FIG 5 Estimation of the HTLV-1 gene copy number in TL-Om1 cells by synchronized qPCR. gDNA of TL-Om1 and Jurkat cells and of PBMCs from two healthy donors was tested for qPCR with synchronous amplification primer sets for HTLV-1, RPPH1, and ALB genes. (A) Construction of control plasmid with a single copy of each target sequence; (B) data indicate C_T scores of HTLV-1, RPPH1, and ALB genes for control plasmid at 1 pg, 100 fg/reaction, and for TL-Om1 and Jurkat cells. qPCR with the plasmid showed synchronous amplification of all primer sets. Each dot indicates the mean from triplicate analyses. The C_T scores in the graph are the results of correction by the factors described in Table 1. (C) Estimated HTLV-1 and ALB gene copy number in TL-Om1 and Jurkat cells. Data were estimated using the difference in C_T scores between target genes and RPPH1 genes.

Additionally, we tried to determine the HTLV-1 copy number in TL-Om1 cells using a synchronized qPCR method. We prepared a plasmid that had one copy of every target PCR amplicon (Fig. 5A). The plasmid had the same copy number as all the target regions. Using the plasmid as a template, we performed qPCR and confirmed the synchronized amplification of primer sets for HTLV-1, RPPH1, and ALB genes (Fig. 5B). The difference in mean C_T scores for the HTLV-1 gene to the RPPH1 gene was 1.05 cycles on average in TL-Om1 cells (Fig. 5C and Table 3). As with the sequencing analysis, use of the synchronized qPCR method also estimated the copy number of the LTR to be 4.01, indicating that TL-Om1 cells have two LTRs (Fig. 5C and Table 3).

Comparison of HTLV-1 copy number from different calculation methods. We compared the results of HTLV-1 and ALB gene copy number obtained from FISH, digital PCR, and synchronized qPCR. The copy number ratios of the HTLV-1 gene to the RPPH1 gene in TL-Om1 cells were 0.46, 0.51, and 0.48, from FISH, digital PCR, and synchronized qPCR, respectively, and those for the ALB gene were 0.76, 0.74, and 0.74 (Fig. 6 and Table 3). The results from these varied assays strongly support one another, indicating that TL-Om1 cells are suitable for use as a reference material for HTLV-1 qPCR.

DISCUSSION

Recently, NAT reference materials have been established for the safety of blood and blood products, such as international standards for HIV, hepatitis B virus, and hepatitis C virus (22–24). These materials have been frequently used for the purpose of calibration and validation of test systems, preparation of secondary reference materials, and comparison of multicenter results, which have helped improve the consistency of the results. Most international standards for blood-transmitted viruses use plasma from infected human blood, because the test target is extracted from human plasma. With regard to HTLV-1 NAT, it may be better to use a cell line as a reference material to standardize the qPCR results, because this test uses cells obtained from peripheral blood. An example of NAT reference material using cell lines is reported in a test for quantitation of BCR-ABL mRNA. Panels of K562 cells combined with HL60 cells were set as standards, which have been approved by the WHO Expert Committee of Biological Standardization (25). Although a variety of cell lines harboring HTLV-1 provirus in their genomes has been established, detailed characterization of the candidate cell lines with regard to their suitability as reference materials for HTLV-1 NATs has not yet been per-

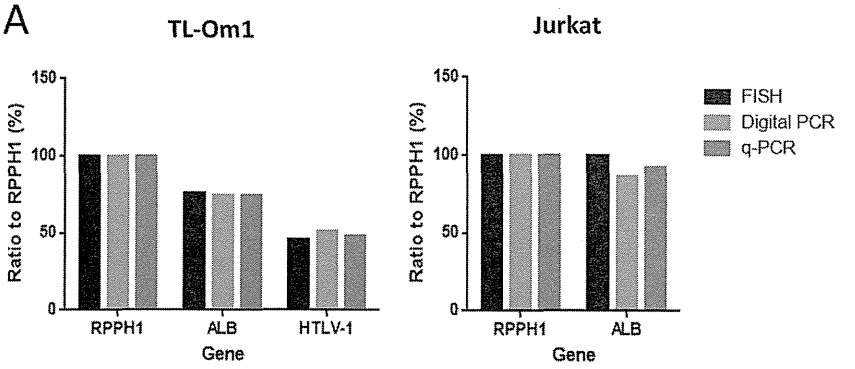

FIG 6 HTLV-1- and ALB-to-RPPH1 gene copy number ratios. (A) Comparison of the HTLV-1- and ALB-to-RPPH1 gene copy number ratios determined by FISH, digital PCR, and qPCR. Data indicate percentages of gene copy number ratio to the RPPH1 gene.

formed. Among the HTLV-1 cell lines, TL-Om1 is well known to be latently infected with HTLV-1 and is thought to be stable for HTLV-1 clonality (17, 26). Transcription from HTLV-1 provirus in TL-Om1 cells is blocked by the highly methylated LTR (27).

In this study, we evaluated the distinct genomic properties of HTLV-1 and IC genes in TL-Om1 cells with regard to their suitability as reference materials for HTLV-1 NATs. Precise information about HTLV-1 infectivity, karyotype, and absolute copy number of HTLV-1 and cellular control genes of TL-Om1 is useful for applying TL-Om1 as a reference material for HTLV-1 qPCR. As such, for this use, TL-Om1 has advantages over other cell lines, such as the human ATL cell line MT2 and the rat T-cell line TARL-2. A recent study of HTLV-1 testing in Japanese blood donor screening revealed that virus prevalence is not limited to areas where HTLV-1 is endemic but has shifted to the entire country, especially the Tokyo metropolitan area (6). Nationwide HTLV-1 tests have been performed on pregnant women in Japan since the end of 2010. The frequent occurrence of seroindeterminate results after Western blotting is one weakness of the HTLV-1 antibody tests. HTLV-1 qPCR is thought to be a solution for decreasing the number of seroindeterminate results; therefore, an accurate measurement of HTLV-1 proviral DNA by qPCR is needed. Additionally, a PVL value of >4% in PBMCs is reported to be a risk factor for ATL development from HTLV-1 asymptomatic carriers, which emphasizes the importance of measuring PVL by qPCR (7). PVL monitoring also provides a risk indicator for HAM/TSP (8).

An attempt to minimize the differences between laboratories by using a common plasmid that included the pX region has been reported. When standard curves were constructed by utilizing the common plasmid in all participating laboratories, the differences in median intralaboratory coefficient of variation (CV) could be reduced by about half (16). Although the attempt worked well among participating laboratories with in-house qPCR methods, the transferability of utilizing common plasmids for standard curves to other methods for PVL determination, for example, digital PCR, is uncertain.

To standardize HTLV-1 qPCR, we advocate the use of TL-Om1 cells with finely elucidated HTLV-1 genomic information as reference material. A previous report showed that PVL values of males and females, on average, are 1.39% and 2.10%, respectively (7). Thus, a dilution or a serial dilution of TL-Om1 with PBMCs or Jurkat cells at a PVL value of around 2% would be an appropriate material for the standardization of HTLV-1 qPCR. These kinds of references can be easily prepared, because the absolute gene copy number is determined from the dilution rate of TL-Om1. TL-Om1 cells were also used as a control in a deep-sequencing-based method for the quantification of the clone size of HTLV-1-infected cells in HTLV-1 carrier or ATL patients (28).

We conclude that TL-Om1 cells can be used as a useful reference material for HTLV-1 NATs. By using TL-Om1 cells, researchers will be able to define the exact values of HTLV-1 by quantifying the copy numbers of provirus and IC genes. In the future, we hope that other laboratories will utilize the features of TL-Om1 cells to standardize the HTLV-1 qPCR.

ACKNOWLEDGMENTS

This work was supported by grants-in-aid for scientific research and by Health and Labor Sciences research grant H23-shinkou-ippan-016 from the Ministry of Health, Labor and Welfare of Japan.

We thank all the members of the HTLV-1 qPCR standardization group for their useful discussions about this research.

We declare that we do not have any competing interests.

Ethical approval was not required for this study.

REFERENCES

1. **Hinuma Y, Nagata K, Hanaoka M, Nakai M, Matsumoto T, Kinoshita KI, Shirakawa S, Miyoshi I.** 1981. Adult T-cell leukemia: antigen in an ATL cell line and detection of antibodies to the antigen in human sera. Proc Natl Acad Sci U S A 78:6476–6480. http://dx.doi.org/10.1073/pnas.78.10.6476.
2. **Poiesz BJ, Ruscetti FW, Gazdar AF, Bunn PA, Minna JD, Gallo RC.** 1980. Detection and isolation of type C retrovirus particles from fresh and cultured lymphocytes of a patient with cutaneous T-cell lymphoma. Proc Natl Acad Sci U S A 77:7415–7419. http://dx.doi.org/10.1073/pnas.77.12.7415.
3. **Watanabe T.** 1997. HTLV-1-associated diseases. Int J Hematol 66:257–278. http://dx.doi.org/10.1016/S0925-5710(97)00077-7.
4. **Gessain A, Cassar O.** 2012. Epidemiological aspects and world distribution of HTLV-1 infection. Front Microbiol 3:388. http://dx.doi.org/10.3389/fmicb.2012.00388.
5. **Watanabe T.** 2011. Current status of HTLV-1 infection. Int J Hematol 94:430–434. http://dx.doi.org/10.1007/s12185-011-0934-4.
6. **Satake M, Yamaguchi K, Tadokoro K.** 2012. Current prevalence of HTLV-1 in Japan as determined by screening of blood donors. J Med Virol 84:327–335. http://dx.doi.org/10.1002/jmv.23181.
7. **Iwanaga M, Watanabe T, Utsunomiya A, Okayama A, Uchimaru K, Koh KR, Ogata M, Kikuchi H, Sagara Y, Uozumi K, Mochizuki M, Tsukasaki K, Saburi Y, Yamamura M, Tanaka J, Moriuchi Y, Hino S, Kamihira S, Yamaguchi K, Joint Study on Predisposing Factors of ATLDi.** 2010. Human T-cell leukemia virus type I (HTLV-1) proviral load

and disease progression in asymptomatic HTLV-1 carriers: a nationwide prospective study in Japan. Blood 116:1211–1219. http://dx.doi.org/10.1182/blood-2009-12-257410.

8. Takenouchi N, Yamano Y, Usuku K, Osame M, Izumo S. 2003. Usefulness of proviral load measurement for monitoring of disease activity in individual patients with human T-lymphotropic virus type I-associated myelopathy/tropical spastic paraparesis. J Neurovirol 9:29–35. http://dx.doi.org/10.1080/13550280390173418.
9. Costa JM, Segurado AC. 2009. Molecular evidence of human T-cell lymphotropic virus types 1 and 2 (HTLV-1 and HTLV-2) infections in HTLV seroindeterminate individuals from Sao Paulo, Brazil. J Clin Virol 44:185–189. http://dx.doi.org/10.1016/j.jcv.2008.12.015.
10. Zanjani DS, Shahabi M, Talaei N, Afzalaghaee M, Tehranian F, Bazargani R. 2011. Molecular analysis of human T cell lymphotropic virus type 1 and 2 (HTLV-1/2) seroindeterminate blood donors from Northeast Iran: evidence of proviral *tax*, *env*, and *gag* sequences. AIDS Res Hum Retroviruses 27:131–135. http://dx.doi.org/10.1089/aid.2010.0017.
11. Watanabe M, Ohsugi T, Shoda M, Ishida T, Aizawa S, Maruyama-Nagai M, Utsunomiya A, Koga S, Yamada Y, Kamihira S, Okayama A, Kikuchi H, Uozumi K, Yamaguchi K, Higashihara M, Umezawa K, Watanabe T, Horie R. 2005. Dual targeting of transformed and untransformed HTLV-1-infected T cells by DHMEQ, a potent and selective inhibitor of NF-kappaB, as a strategy for chemoprevention and therapy of adult T-cell leukemia. Blood 106:2462–2471. http://dx.doi.org/10.1182/blood-2004-09-3646.
12. Tanaka G, Okayama A, Watanabe T, Aizawa S, Stuver S, Mueller N, Hsieh CC, Tsubouchi H. 2005. The clonal expansion of human T lymphotropic virus type 1-infected T cells: a comparison between seroconverters and long-term carriers. J Infect Dis 191:1140–1147. http://dx.doi.org/10.1086/428625.
13. Nagai M, Yamano Y, Brennan MB, Mora CA, Jacobson S. 2001. Increased HTLV-I proviral load and preferential expansion of HTLV-I Tax-specific CD8+ T cells in cerebrospinal fluid from patients with HAM/TSP. Ann Neurol 50:807–812. http://dx.doi.org/10.1002/ana.10065.
14. Kamihira S, Dateki N, Sugahara K, Yamada Y, Tomonaga M, Maeda T, Tahara M. 2000. Real-time polymerase chain reaction for quantification of HTLV-1 proviral load: application for analyzing aberrant integration of the proviral DNA in adult T-cell leukemia. Int J Hematol 72:79–84.
15. Ueno S, Umeki K, Takajo I, Nagatomo Y, Kusumoto N, Umekita K, Morishita K, Okayama A. 2012. Proviral loads of human T-lymphotropic virus type 1 in asymptomatic carriers with different infection routes. Int J Cancer 130:2318–2326. http://dx.doi.org/10.1002/ijc.26289.
16. Kamihira S, Yamano Y, Iwanaga M, Sasaki D, Satake M, Okayama A, Umeki K, Kubota R, Izumo S, Yamaguchi K, Watanabe T. 2010. Intra- and inter-laboratory variability in human T-cell leukemia virus type-1 proviral load quantification using real-time polymerase chain reaction assays: a multi-center study. Cancer Sci 101:2361–2367. http://dx.doi.org/10.1111/j.1349-7006.2010.01720.x.
17. Sugamura K, Fujii M, Kannagi M, Sakitani M, Takeuchi M, Hinuma Y. 1984. Cell surface phenotypes and expression of viral antigens of various human cell lines carrying human T-cell leukemia virus. Int J Cancer 34:221–228. http://dx.doi.org/10.1002/ijc.2910340213.
18. Yoshida M, Seiki M, Yamaguchi K, Takatsuki K. 1984. Monoclonal integration of human T-cell leukemia provirus in all primary tumors of adult T-cell leukemia suggests causative role of human T-cell leukemia virus in the disease. Proc Natl Acad Sci U S A 81:2534–2537. http://dx.doi.org/10.1073/pnas.81.8.2534.
19. Yamaguchi K, Seiki M, Yoshida M, Nishimura H, Kawano F, Takatsuki K. 1984. The detection of human T cell leukemia virus proviral DNA and its application for classification and diagnosis of T cell malignancy. Blood 63:1235–1240.
20. Uren AG, Mikkers H, Kool J, van der Weyden L, Lund AH, Wilson CH, Rance R, Jonkers J, van Lohuizen M, Berns A, Adams DJ. 2009. A high-throughput Splinkerette-PCR method for the isolation and sequencing of retroviral insertion sites. Nat Protoc 4:789–798. http://dx.doi.org/10.1038/nprot.2009.64.
21. Sanger F, Nicklen S, Coulson AR. 1977. DNA sequencing with chain-terminating inhibitors. Proc Natl Acad Sci U S A 74:5463–5467. http://dx.doi.org/10.1073/pnas.74.12.5463.
22. World Health Organization. 2011. International collaborative study to establish the 3rd WHO international standard for HIV-1 NAT assays. WHO ECBS report 2011 WHO/BS/2011.2178. WHO, Geneva, Switzerland.
23. Fryer JF, Heath A, Wilkinson DE, Minor PD, The Collaborative Study Group. 2011. Collaborative study to evaluate the proposed 3rd WHO international standard for hepatitis B virus (HBV) for nucleic acid amplification technology (NAT)-based assays. WHO ECBS report 2011 WHO/BS/2011.2170. WHO, Geneva, Switzerland.
24. Fryer JF, Heath A, Wilkinson DE, Minor PD, The Collaborative Study Group. 2011. Collaborative study to evaluate the proposed 4th WHO international standard for hepatitis C virus (HCV) for nucleic acid amplification technology (NAT)-based assays. WHO ECBS report 2011 WHO/BS/2011.2173. WHO, Geneva, Switzerland.
25. White HE, Matejtschuk P, Rigsby P, Gabert J, Lin F, Lynn Wang Y, Branford S, Muller MC, Beaufils N, Beillard E, Colomer D, Dvorakova D, Ehrencrona H, Goh HG, El Housni H, Jones D, Kairisto V, Kamel-Reid S, Kim DW, Langabeer S, Ma ES, Press RD, Romeo G, Wang L, Zoi K, Hughes T, Saglio G, Hochhaus A, Goldman JM, Metcalfe P, Cross NC. 2010. Establishment of the first World Health Organization international genetic reference panel for quantitation of BCR-ABL mRNA. Blood 116:e111–e117. http://dx.doi.org/10.1182/blood-2010-06-291641.
26. Koiwa T, Hamano-Usami A, Ishida T, Okayama A, Yamaguchi K, Kamihira S, Watanabe T. 2002. 5′-Long terminal repeat-selective CpG methylation of latent human T-cell leukemia virus type 1 provirus *in vitro* and *in vivo*. J Virol 76:9389–9397. http://dx.doi.org/10.1128/JVI.76.18.9389-9397.2002.
27. Ishida T, Hamano A, Koiwa T, Watanabe T. 2006. 5′ Long terminal repeat (LTR)-selective methylation of latently infected HIV-1 provirus that is demethylated by reactivation signals. Retrovirology 3:69. http://dx.doi.org/10.1186/1742-4690-3-69.
28. Firouzi S, Lopez Y, Suzuki Y, Nakai K, Sugano S, Yamochi T, Watanabe T. 2014. Development and validation of a new high-throughput method to investigate the clonality of HTLV-1-infected cells based on provirus integration sites. Genome Med 6:46. http://dx.doi.org/10.1186/gm568.

J Neuropathol Exp Neurol

Vol. 74, No. 1
January 2015
pp. 2–14

ORIGINAL ARTICLE

OPEN

Visualization of HTLV-1–Specific Cytotoxic T Lymphocytes in the Spinal Cords of Patients With HTLV-1–Associated Myelopathy/Tropical Spastic Paraparesis

Eiji Matsuura, MD, PhD, Ryuji Kubota, MD, PhD, Yuetsu Tanaka, MD, PhD, Hiroshi Takashima, MD, PhD, and Shuji Izumo, MD, PhD

Abstract

Activated human T-lymphotropic virus type-1 (HTLV-1)–specific CD8-positive cytotoxic T lymphocytes (CTLs) are markedly increased in the periphery of patients with HTLV-1–associated myelopathy/tropical spastic paraparesis (HAM/TSP), an HTLV-1–induced inflammatory disease of the CNS. Although virus-specific CTLs play a pivotal role to eliminate virus-infected cells, the potential role of HTLV-1–specific CTLs in the pathogenesis of HAM/TSP remains unclear. To address this issue, we evaluated the infiltration of HTLV-1–specific CTLs and the expression of HTLV-1 proteins in the spinal cords of 3 patients with HAM/TSP. Confocal laser scanning microscopy with our unique staining procedure made it possible to visualize HTLV-1–specific CTLs infiltrating the CNS of the HAM/TSP patients. The frequency of HTLV-1–specific CTLs was more than 20% of CD8-positive cells infiltrating the CNS. In addition, HTLV-1 proteins were detected in CD4-positive infiltrating T lymphocytes but not CNS resident cells. Although neurons were generally preserved, apoptotic oligodendrocytes were frequently in contact with CD8-positive cells; this likely resulted in demyelination. These findings suggest that the immune responses of the CTLs against HTLV-1–infected CD4-positive lymphocytes migrating into the CNS resulted in bystander neural damage.

Key Words: Apoptosis, Cytotoxic T lymphocyte, Demyelination, HTLV-1–associated myelopathy/tropical spastic paraparesis (HAM/TSP), Human T-lymphotropic virus type-1 (HTLV-1).

From the Department of Neurology and Geriatrics (EM, HT) and Center for Chronic Viral Diseases (RK, SI), Kagoshima University Graduate School of Medical and Dental Sciences, Kagoshima; and Department of Immunology, University of the Ryukyus, Okinawa (YT), Japan.

Send correspondence and reprint requests to: Ryuji Kubota, MD, PhD, Center for Chronic Viral Diseases, Kagoshima University Graduate School of Medical and Dental Sciences, 8-35-1 Sakuragaoka, Kagoshima 890-8544, Japan; E-mail: kubotar@m2.kufm.kagoshima-u.ac.jp

This work was supported by Health and Labour Sciences Research Grants from the Ministry of Health, Labour and Welfare of Japan and JSPS KAKENHI Grants 25293205 and 24133701 from the Ministry of Education, Culture, Sports, Science, and Technology of Japan.

The authors declare no conflict of interest.

Supplemental digital content is available for this article. Direct URL citations appear in the printed text and are provided in the HTML and PDF versions of this article on the journal's Web site (www.jneuropath.com).

INTRODUCTION

Human T-lymphotropic virus type 1 (HTLV-1) infection is estimated to affect 1 to 2 × 10^7 people worldwide. Although HTLV-1 infection is lifelong, the majority of infected individuals remain asymptomatic; only 1% to 2% of these individuals develop HTLV-1–associated diseases, including adult T-cell leukemia/lymphoma (1), and a range of chronic inflammatory diseases, including myelopathy (2–4), uveitis (5), arthritis (6), polymyositis (7, 8), inclusion-body myositis (9, 10), and alveolitis (11). The most recognized inflammatory disease is HTLV-1–associated myelopathy/tropical spastic paraparesis (HAM/TSP), in which CNS lesions correspond to progressive weakness of the lower extremities, with spasticity, urinary incontinence, and mild sensory disturbance. Patients with HAM/TSP exhibit higher HTLV-1 proviral load in the peripheral blood mononuclear cells (PBMCs) than asymptomatic HTLV-1 carriers (12). Furthermore, HTLV-1–infected cells accumulate in the cerebrospinal fluid (CSF) on neurologic exacerbation (13). One of the most striking features of the cellular immune response in patients with HAM/TSP is the highly elevated numbers of HTLV-1–specific CD8-positive cytotoxic T lymphocytes (CTLs) in PBMCs compared with asymptomatic HTLV-1 carriers (14, 15). These CTLs produce proinflammatory cytokines (16, 17). The HTLV-1–specific CTLs are thought to be a key factor in the pathogenesis of HAM/TSP (18, 19). This persistently activated CTL immune response to HTLV-1 provides unequivocal evidence of persistent HTLV-1 antigen expression in vivo. To date, no previous studies have shown CTLs and HTLV-1 proteins in CNS tissues from patients with HAM/TSP.

Although Skinner et al visualized antigen-specific T cells with nonfrozen tissues (20), the method has not been adapted to frozen tissue samples. In this study, we established novel in situ staining methods for detecting virus-specific CTLs and HTLV-1 proteins in frozen human tissue samples. We detected a number of HTLV-1–specific CTLs and HTLV-1–infected CD4-positive cells infiltrating the CNS and verified the bystander hypothesis that the interaction between HTLV-1–specific CTLs and HTLV-1–infected T lymphocytes causes damage to bystander neural cells in the CNS (21).

MATERIALS AND METHODS

Subjects

We obtained autopsied spinal cord tissue from 9 HAM/TSP patients after obtaining written informed consent from their

TABLE 1. Patient Clinical Data

Patient ID	Age, years/Sex	Duration of Illness, years	Cause of Death	Cellular Infiltration[a]	Human T-Lymphotropic Virus Type-1 Antibody Titer[b]	HLA[c]
8624	59/Male	7	Pulmonary tuberculosis	3+	512×	A*02 + A*24-
6315	71/Female	4.5	Bacterial pneumonia	3+	32,768×	A*02-A*24+
6664	52/Female	8	Pontine hemorrhage	1+	131,072×	A*02 + A*24+

[a] Cellular infiltration: a degree of cellular infiltration in the spinal cord.
[b] The antibody titer in serum was determined by particle agglutination method.
[c] HLA: human leukocyte antigen.

family members and stored them at −80°C until use. Human T-lymphotropic virus type 1 Tax11-19 (LLFGYPVYV) and Tax301-309 (SFHSLHLLF) are well-characterized immunodominant epitopes that are restricted to HLA-A*02 and HLA-A*24, respectively (22, 23). Human leukocyte antigen (HLA) typing was performed in all of the autopsied samples (24). Three samples were found suitable for use in this study. The first was from an HLA-A*02–positive patient (No. 8624), the second was from an HLA-A*24–positive patient (No. 6315), and the third was from an HLA-A*02 and HLA-A*24 double–positive patient (No. 6664). We had frozen block samples from entire levels of the spinal cord of each patient. We first evaluated each block by routine histology and used the samples with inflammatory lesions for the study. The clinical characteristics of the patients are shown in Table 1. This study was approved by the Kagoshima University Ethics Committee.

Immunohistochemistry

Primary and secondary antibodies are listed in Table 2. Fresh-frozen spinal cord samples were cut into 8-μm-thick sections, placed on aminosilane-coated slides, and dried for 3 hours. After fixation with 4% paraformaldehyde (PFA) in PBS for 20 minutes at room temperature (RT), the sections were incubated with a primary monoclonal antibody (mAb) for 60 minutes at RT. The samples were washed with PBS after each step.

For immunohistochemistry, the sections were treated with 3% H_2O_2 in PBS for 20 minutes and subsequently incubated with horseradish peroxidase–labeled polymer-conjugated anti-mouse antibody (Ab) reagent (EnVision+ reagent; Dako, Tokyo, Japan) for 30 minutes at RT. Finally, peroxidase was visualized using 3-amino-9-ethylcarbazole (AEC) substrate as the red color. The sections were counterstained with hematoxylin and analyzed by light microscopy.

For immunofluorescence staining, the sections were incubated with fluorescence-conjugated secondary antibodies for 60 minutes at RT in the dark. The sections were counterstained with 4′,6-diamidino-2-phenylindole (DAPI) and analyzed using a confocal laser scanning microscope (FV500; Olympus, Tokyo, Japan). For double staining, 2 primary antibodies with

TABLE 2. Primary and Secondary Antibodies Used for Immunohistochemical Studies

Antibody	Dilution	Company
Mouse anti-CD4 mAb (4B12, IgG1)	50×	Dako, Tokyo, Japan
Rat anti-CD4 mAb (YNB46.1.8, IgG)	50×	Abcam, Tokyo, Japan
Mouse anti-CD3 mAb (UCHT1, IgG1)	50×	Beckman Coulter, Tokyo, Japan
Mouse anti-CD8 mAb (DK25, IgG1)	50×	Dako
Mouse anti-CD68 mAb (KP-1, IgG1)	400×	Dako
Mouse anti–HTLV-1 Tax mAb (Lt-4, IgG3)	250×	Not applicable*
Mouse anti–HTLV-1 Gag mAb (TP-7, IgG1)	400×	Abcam
Mouse anti–HTLV-1 Env mAb (65/6C2, IgG1)	2000×	Abcam
Rabbit anti–Ki-67 Ab (IgG)	100×	Abcam
Mouse anti–granzyme B mAb (GB11, IgG1)	50×	Serotec, Kidlington, UK
Mouse anti–IFN-γ mAb (45.15, IgG1)	500×	Ancell, Bayport, MN
Mouse anti-CNPase mAb (11-5B, IgG1)	400×	Millipore, Tokyo, Japan
Mouse anti-GFAP mAb (6 F2, IgG1)	250×	Dako
Mouse anti-perforin mAb (δG9, IgG2b)	200×	BioVision, Milpitas, CA
Rabbit anti-PE Ab	500×	BioGenesis, Westminster, CO
Rabbit anti–active caspase-3 mAb (E83-77, IgG)	50×	Epitomics, Burlingame, CA
Rabbit anti–single-stranded DNA (ss DNA) Ab (F7-26)	50×	Abcam
Alexa Fluor 488-, 594- or 647–conjugated goat anti-mouse IgG1 or IgG3 Abs	1000×	Invitrogen, Tokyo, Japan
Alexa Fluor 488–conjugated goat anti-rabbit IgG Ab	1000×	Invitrogen
Alexa Fluor 488–conjugated goat anti-rat IgG Ab	1000×	Invitrogen

*Described in Lee et al (25).
Ab, antibody; CNPase, 2′,3′-cyclic-nucleotide 3′-phosphodiesterase; GFAP, glial fibrillary acidic protein; HTLV-1, human T-lymphotrophic virus-1; IFN-γ, interferon-γ; mAb, monoclonal antibody.

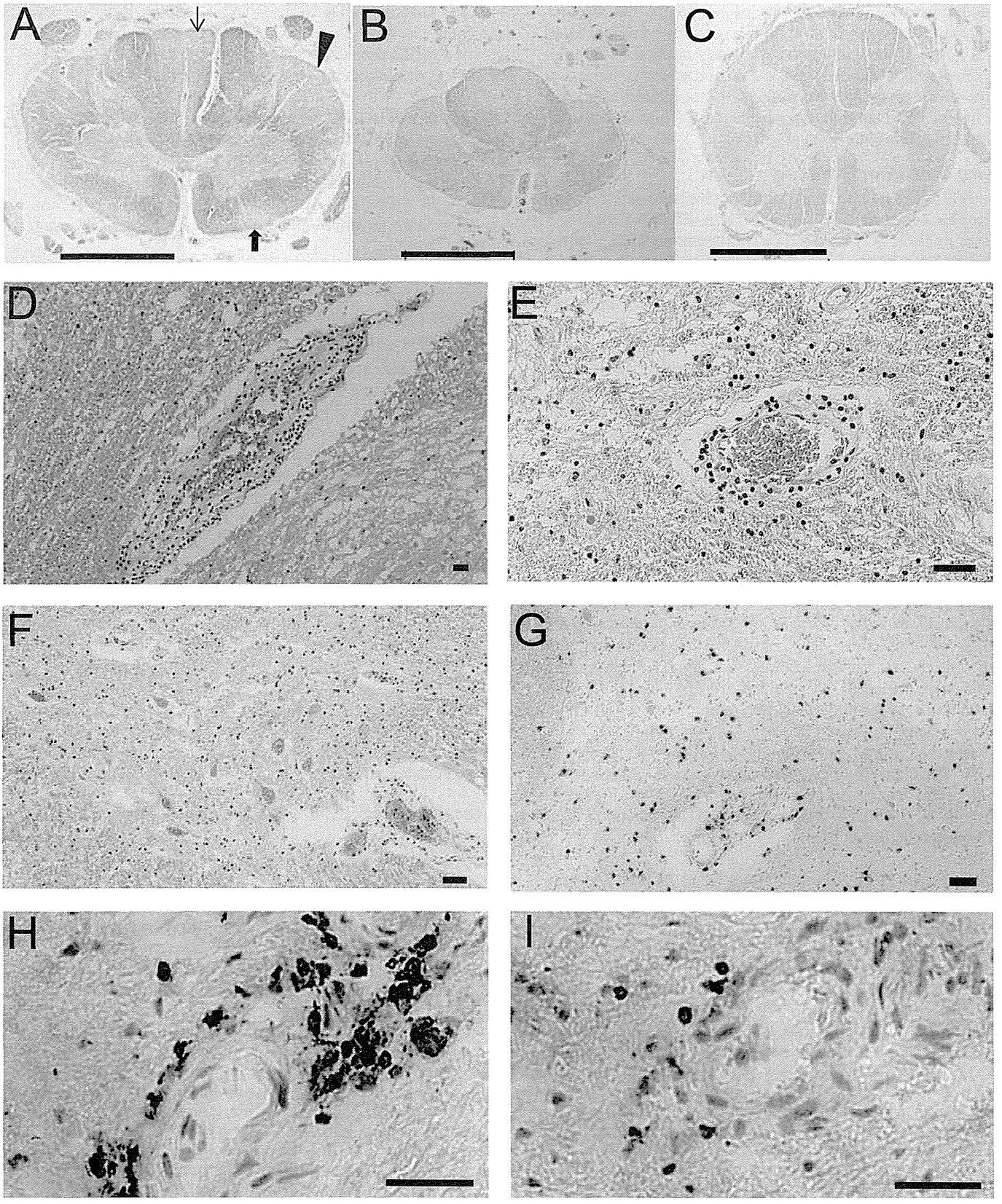

different immunoglobulin subclasses reacted to the sections simultaneously overnight at 4°C. The sections were incubated with 2 Alexa Fluor–conjugated secondary antibodies for relevant immunoglobulin subclasses. For multicolor staining, we always obtained images by sequentially scanning with each laser line to avoid the fluorescence bleeding. The sections were evaluated by 2 investigators.

In Situ Tetramer Staining

HTLV-1 Tax–specific T lymphocytes were detected with either phycoerythrin (PE)-labeled HLA-A*0201/Tax11-19-tetramer or HLA-A*2402/Tax301-309-tetramer (MBL, Japan) diluted to 1.0 μg/mL. HLA-A*0201/Tax11-19-pentamer was also used to corroborate the results of the tetramer in the staining of the CNS. Phycoerythrin-labeled HLA-A*0201/HIV Gag peptide (SLYNTVATL) tetramer or PE-labeled HLA-A*2402/HIV Env peptide (RYLKDQQLL) tetramer was used as an irrelevant control. The sections were fixed with PBS-buffered 0.1% PFA for 10 minutes and washed with PBS after each step. The sections were incubated with tetramer overnight at 4°C in the presence of proteinase inhibitors (Roche, Tokyo, Japan) and subsequently fixed again with PBS-buffered 4% PFA for 20 minutes at RT. Rabbit anti-PE Ab (500×; BioGenesis, Westminister, CO) was used as the secondary Ab and incubated with the sections for 60 minutes at RT. The signal was enhanced with the EnVision+ system and visualized with AEC chromogen. For immunofluorescence staining, the sections were incubated with goat anti-rabbit Ab labeled with Alexa Fluor 488 for 60 minutes at RT. For double staining, sections were simultaneously incubated with any of anti-CD8 mAb, anti–granzyme B mAb, anti–interferon-γ (IFN-γ) mAb, or Lt-4 mAb and with Tax-tetramer. After overnight incubation and fixation, the sections were incubated with rabbit anti-PE Ab for 60 minutes. The sections were then incubated with Alexa Fluor 594–conjugated anti–mouse IgG1 or IgG3 Ab and Alexa Fluor 488–conjugated goat anti-rabbit IgG Ab for 60 minutes at RT. 4′,6-Diamidino-2-phenylindole was used for counterstaining. To determine the frequency of Tax-tetramer–positive cells among the CD8-positive cells, we counted the cells under full-field observation (400×).

Detection of HTLV-1–Infected Cells in the Tissues

Fresh-frozen spinal cord sections were used to detect HTLV-1 proteins. The sections were dried and fixed with 4% PFA for 20 minutes at RT. Anti–HTLV-1 Tax mAb (Lt-4), anti–HTLV-1 Gag mAb (TP-7), or anti–HTLV-1 Env mAb (65/6C2) was applied to the sections in combination with anti-CD3 mAb, anti-CD4 mAb, or anti–Ki-67 Ab. After the sections were incubated overnight at 4°C, they were incubated with isotype-specific secondary antibodies for 60 minutes at RT in the dark and subsequently counterstained with DAPI.

Detection of Apoptotic Cells

Apoptotic cells were detected with anti–active caspase-3 Ab or anti–single-stranded DNA Ab by light microscopy and confocal laser scanning microscopy. The cells were also detected with TdT-mediated dUTP nick end labeling method according to the manufacturer's instructions (ApopTag Millipore, Billerica, MA).

RESULTS

General Findings in the CNS of HAM/TSP Patients

Transverse sections of the spinal cords of HAM/TSP patients demonstrated atrophy in the lateral columns with thickened meninges (Fig. 1A–C). Symmetric patchy myelin pallor in Luxol fast blue staining was observed in the affected long tracts, lateral cerebrospinal fasciculus, ventral and dorsal spinocerebellar fasciculi, spinothalamic fasciculus in the lateral column, and fasciculus gracilis in the posterior columns. The essential histopathologic feature was a chronic progressive inflammatory process with marked parenchymal exudation of lymphocytes and macrophages around the vessels (i.e. postcapillary venules) in both the gray and white matter of the spinal cord (Fig. 1D, E). The degree of cellular infiltration was strong in Patients 6315 and 8624, whereas Patient 6664 had no significant cell infiltrates (Table 1). Neurons in the anterior horns were generally preserved (Fig. 1F). Immunohistochemical staining of the spinal cord revealed remarkable infiltration of CD8-positive cells (Fig. 1G, H) and CD4-positive cells (Fig. 1I) and macrophages (data not shown) throughout the parenchyma, especially in perivascular areas. These histochemical findings are consistent with previous reports.

Detection of HTLV-1 Tax–Specific CTLs in the CNS

To validate the in situ tetramer staining procedure for visualization of HTLV-1–specific CTLs, PBMCs of HLA-A*02–positive patients with HAM/TSP were fixed on slides and stained with HLA-A*02/Tax11-19 tetramer and anti-CD8 mAb. The fluorescence pattern of the tetramer exactly colocalized with that of anti-CD8 mAb on the PBMCs (Fig. 2A). This is consistent with the fact that CD8 cells express a T-cell

FIGURE 1. Routine and histochemical study of spinal cords from patients with HTLV-1–associated myelopathy/tropical spastic paraparesis (HAM/TSP) by light microscopy. **(A–C)** The spinal cord (**A**, cervical level; **B**, lower thoracic level; **C**, lumbar level) of a HAM/TSP patient shows marked atrophy in the lateral columns; original magnification is 40×. The bars indicate 3 mm. **(A)** Symmetric myelin pallor is noted in the lateral cerebrospinal fasciculus, ventral and dorsal spinocerebellar fasciculus, lateral spinothalamic fasciculus in the lateral column (arrowhead), anterior spinothalamic fasciculus in the anterior column (thick arrow), and fasciculus gracilis in the posterior column (thin arrow). **(B)** There is marked atrophy, particularly of the lateral column. **(C)** Mild atrophy in the lumbar level. **(D)** A number of infiltrating cells are scattered throughout the section of the spinal cord. **(E)** Perivascular and parenchymal mononuclear cell infiltrates. **(F)** Neurons in the anterior horn are fairly preserved in the atrophied spinal cord. **(G, H)** Immunohistochemical study revealed that markedly infiltrating CD8-positive cells (red) are scattered in the parenchyma and around a small vessel in the spinal cord. **(I)** CD4-positive cells (red) are observed around a small vessel in the spinal cord. Nuclei were counterstained with hematoxylin (**D–I**, blue). Scale bar = 100 μm. **(A–C)** Luxol fast blue; **(D–F)** hematoxylin and eosin; **(G–I)** immunohistochemistry with hematoxylin counterstain.

receptor. We could not detect HTLV-1–specific CTLs at all with Tax-tetramer or -pentamer in frozen samples using a reported procedure for nonfrozen samples (20). We tested several modified staining procedures and finally found that prefixing the frozen sections at a very low concentration of PFA was optimal. We selected the sections that stained best with the tetramer or pentamer from several sections from each block. We detected HTLV-1 Tax11-19–specific CTLs in the parenchyma of the spinal cords from an HLA-A*02–positive patient (Fig. 2B) and an HLA-A*24–positive patient (Fig. 2C) with HLA-A*02/Tax-tetramer and HLA-A*24/Tax-tetramer, respectively. The CTLs were also detected in the thickened leptomeninges (Fig. 2D). On the other hand, no cells were detected by HIV Gag-tetramer and influenza-tetramer as tetramer controls (Fig. 2E).

Accumulation of HTLV-1 Tax–Specific CD8-positive CTLs in the CNS

To determine the frequency of HTLV-1 Tax–specific CTLs in CD8-positive lymphocytes infiltrating the CNS, we performed double staining for HTLV-1 Tax–specific CTLs and CD8-positive lymphocytes. Tax-specific CTLs stained with Tax-tetramer were frequently noted in the lesions. Double staining revealed that the fluorescence of Tax-tetramer colocalized with that of anti-CD8 mAb in all 3 patients (Fig. 3A–C). Meanwhile, HIV-tetramer restricted by either HLA-A*02 or HLA-A*24 did not bind any CD8-positive cells in the corresponding specimen (Fig. 3D). Next, we evaluated the frequency of Tax-specific CTLs in CD8-positive lymphocytes in 4 sections of the spinal cord from each patient. The percentages of Tax-specific CTLs in CD8-positive cells were 22.1% (62 of 280) and 31.1% (96 of 309) in patients with HLA-A*02–positive and HLA-A*24–positive patients, respectively (Table 3). Patient 6664 had no significant cellular infiltrates, and we only detected 2 HLA-A*24/Tax-tetramer–positive and no HLA-A*02/Tax-tetramer–positive cells in the 4 sections of the spinal cord from that patient. In addition to Tax-tetramer, Tax-pentamer was also used for the staining of the tissues from Patient 8624 to corroborate our results with Tax-tetramer. Similarly, the fluorescence of Tax-pentamer exactly colocalized with that of anti-CD8 mAb; the frequency of Tax-pentamer–positive cells in CD8-positive cells was 31% in the lesion (Fig. 3E).

Detection of HTLV-1 Proteins in the CNS

Although the HTLV-1 gene has been detected in CD4-positive lymphocytes, its viral protein has not been detected in freshly isolated lymphocytes. Therefore, we used HTLV-1–infected cell lines in a preliminary study for visualizing HTLV-1 Tax protein. Detected HTLV-1 Tax showed a patchy staining pattern in the nuclei of a human cell line (Figure, Supplemental Digital Content 1, parts A and B, http://links.lww.com/NEN/A676). Although HTLV-1 Tax was not detected in noncultured PBMCs, we detected the protein in PBMCs of patients with HAM/TSP after 8-hour culture (Figure, Supplemental Digital Content 1, part C, http://links.lww.com/NEN/A676).

We next detected 3 HTLV-1 proteins (Tax, Env, and Gag) in the CNS tissues of the HAM-TSP patients. Tax was found in the cells near vessels (Fig. 4A, B) and in the leptomeninges. The nuclear protein Tax showed a patchy staining pattern in the nuclei (Fig. 4C, D, G), whereas Env and Gag were detected in the cell membrane or cytoplasm (Fig. 4E–G). Double staining revealed that the cells expressing Tax, Env, or Gag were CD4-positive lymphocytes (Fig. 4C–F). CD68-, CD8-, CNPase-, and glial fibrillary acidic protein (GFAP)–positive cells were not positive for HTLV-1 Tax (Figure, Supplemental Digital Content 2, http://links.lww.com/NEN/A677). To investigate whether HTLV-1–infected cells proliferate in the CNS, we stained with anti-Tax mAb and anti–Ki-67 Ab (a marker of cell proliferation); however, Ki-67–positive Tax-positive cells were very rare; we detected only 2 cells in the 2 sections (data not shown). To investigate the frequency of HTLV-1–infected cells in the CD4-positive population and the frequency of apoptotic cells in HTLV-1–infected cells, we performed triple staining for CD4, active caspase-3, and HTLV-1 Env protein. The HTLV-1–positive cells in infiltrating CD4-positive cells were 60.3% and 82.4% in Patients 8624 and 6315, respectively (Table 3). More than 50% of infiltrating CD4-positive cells were infected with HTLV-1. Furthermore, HTLV-1–infected cells had a greater tendency to undergo apoptosis than noninfected cells; 36.4% of the infected cells were undergoing apoptosis, whereas 10.3% of noninfected cells were undergoing apoptosis in Patient 8624 (Table 3). Because the sample from Patient 6664 showed only a few cellular infiltrates, we could not evaluate the frequency of apoptosis in that case.

Functional Molecules of HTLV-1–Specific CD8-Positive CTLs

To investigate whether HTLV-1 Tax–specific CD8-positive CTLs have the ability to attack HTLV-1–infected CD4-positive cells in the CNS, we attempted to detect functional molecules of CTLs in the CNS. Granzyme B–, perforin-, and IFN-γ–positive cells were detected in both parenchymal and perivascular areas (Fig. 5A–C). Some of the cells stained with Tax-tetramer were positive for granzyme B (Fig. 5D). Furthermore, double staining revealed that CD8-positive cells sometimes were in contact with HTLV-1–infected cells (Fig. 5E), and that some HTLV-1 Tax–specific CTLs were next to HTLV-1–infected cells in the parenchyma (Fig. 5F). Human T-lymphotropic virus type-1 Tax–specific CTLs were not positive for Ki-67 (data not shown).

Apoptotic Cells

Next, we determined which cells underwent apoptosis in the CNS of the patients. Active caspase-3–positive cells (apoptotic cells) were frequently observed near CD8-positive cells in the parenchyma of the spinal cord, and some of them were in contact with CD8-positive cells (Fig. 5G–I). Active caspase-3 showed granular staining patterns in our pictures, although it has shown a diffuse cytoplasmic pattern in previous studies. The staining pattern may differ because of the different conditions of the frozen samples. We tried to detect the apoptotic cells with formalin-fixed paraffin-embedded samples by light microscopy. Caspase-3 was detected in the cell cytoplasm in those samples (Fig. 6A). Next, we stained the sections by methods other than the anti–active caspase-3 Ab to corroborate

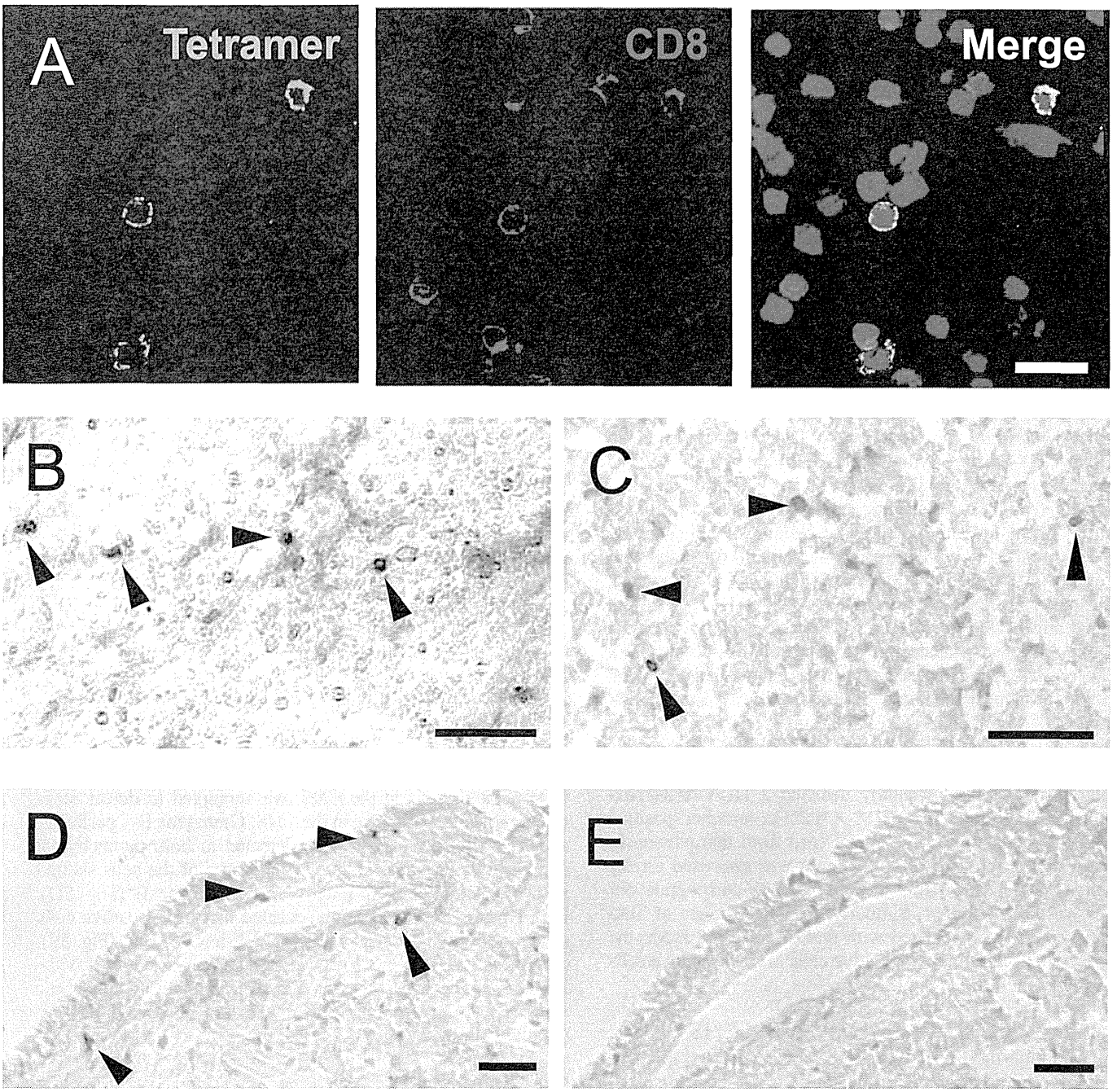

FIGURE 2. Detection of CD8-positive human T-lymphotropic virus type-1 (HTLV-1) Tax–specific cytotoxic T lymphocytes (CTLs) in peripheral blood mononuclear cells (PBMCs) and CNS. **(A)** Double staining with anti-CD8 monoclonal antibody (red) and HLA-A*0201/Tax11-19 or HLA-A*2402/Tax11-19 tetramer (green) was performed with confocal laser scanning microscopy (CLSM). DAPI (blue) was used for counterstaining the nuclei. The 3 colors were captured sequentially using CLSM. Merged images are shown on the right. PBMCs from a patient with HAM/TSP are stained with the tetramer. **(B)** HLA-A*0201/Tax11-19-tetramer–positive cells are scattered in the spinal cord parenchyma (Patient 8624). **(C)** HLA-A*2402/Tax301-309-tetramer–positive cells are seen in the parenchyma of the spinal cord (Patient 6315). **(D)** Cells stained with HLA-A*0201/Tax11-19-tetramer are found around the vessel in the spinal cord leptomeninges (Patient 8624) (red). **(E)** No cells are stained with HLA-A*0201/HIV Gag-tetramer in the adjacent serial section. White and black bars indicate 20 μm and 100 μm, respectively.

the frequent apoptosis in the spinal cord. Using a TdT-mediated dUTP nick end labeling assay, we detected a number of apoptotic cells (Fig. 6B, C). We also stained these spinal cord samples with anti–single-stranded DNA Ab and obtained similar findings (Fig. 6E). Altogether, the 3 staining methods showed frequent apoptosis in the affected spinal cords (Fig. 6).

Double staining revealed that apoptotic cells were CD4-positive or CD68-positive cells (Fig. 7D, E). Interestingly,

oligodendrocytes, which were stained with anti-CNPase mAb (Fig. 7B), were frequently undergoing apoptosis (Fig. 7F). This finding is consistent with the occurrence of demyelination in the spinal cords of HAM/TSP patients. However, oligodendrocytes were not stained with anti–HTLV-1 Tax mAb (data not shown) or anti–HLA-ABC Ab (Fig. 7G). Astrocytes that were stained with anti-GFAP mAb were diffusely distributed throughout the parenchyma (Fig. 7A), whereas GFAP-positive cells

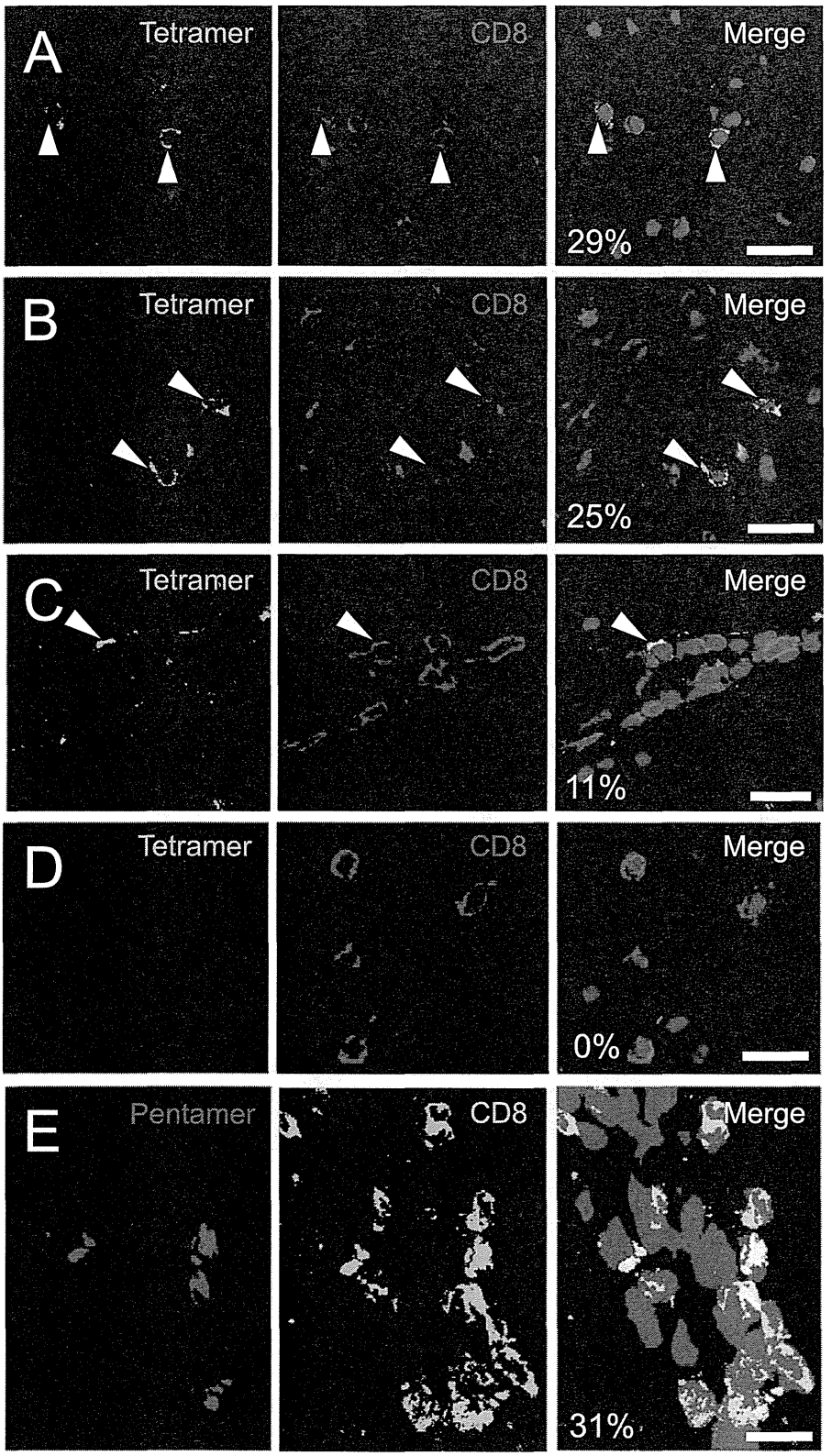

TABLE 3. Cytotoxic T Lymphocytes, Human T-Lymphotrophic Virus-1–Infected Cells and Apoptotic Cells in the CNS

Patient ID	Tax-Specific CTLs in CD8-Positive Cells	Env-Positive Cells in CD4-Positive Cells	Caspase-3–Positive Cells in CD4-Positive Cells	Caspase-3–Positive Cells in Env-Positive CD4-Positive Cells	Caspase-3–Positive Cells in Env-Negative CD4-Positive Cells
8624	22.1% (62/280)*	60.3% (44/73)	26.0% (19/73)	36.4% (16/44)	10.3% (3/29)
6315	31.1% (96/309)	82.4% (103/125)	12.0% (15/125)	12.6% (13/103)	9.1% (2/22)
6664	N/A†	N/A	N/A	N/A	N/A

*The numbers of positive cells/total cells are indicated within parentheses.
†Not applicable; cell infiltration was not significant for evaluation.
CTL, cytotoxic T lymphocytes.

were not positive for active caspase-3 (Fig. 7H). Neurons identified by their size as well as several particles within the neuronal body induced strong autofluorescence but were not positive for active caspase-3 (data not shown).

DISCUSSION

One of the most striking features of the cellular immune responses in patients with HAM/TSP is the highly increased numbers of HTLV-1–specific CTLs in PBMCs and CSF (14, 15); however, little is known about CTLs in the CNS. The fixation of human CNS samples with a very low concentration of PFA made it possible to visualize antigen-specific CTLs using tetramers or a pentamer in the CNS. Strikingly, their frequency reached more than 20% in CD8-positive cells that had migrated to the CNS. In a flow cytometric study in our cohort, we detected HTLV-1 Tax11-19–specific and HTLV-1 Tax301-309–specific CTLs in PBMCs from patients with HAM/TSP at 2.25% (0.0%–18.7%) (26) and 4.34% (0.2%–17.6%) (unpublished data), respectively. The present data are consistent with another report in which the frequency of HTLV-1 Tax–specific CTLs was higher in CSF than in PBMCs (18). Although the frequency of the CTLs differs by the case, it may be attributed to the difference in the phase of the disease or the duration of the illness.

Granzyme B and perforin, both known as cytotoxic molecules of CTLs, were detected along with IFN-γ in the parenchyma near the vessels in the CNS. Some CTLs contained granzyme B. Human T-lymphotropic virus type-1–specific CTLs were in contact with HTLV-1–infected cells, and apoptotic cells were frequently noted near the CD8-positive cells. These results strongly suggest that the infiltrating CTLs function as effector cells in the CNS. Interestingly, a considerable number of oligodendrocytes underwent apoptosis in the affected lesions. Meanwhile, the oligodendrocytes neither increase the expression levels of HLA-ABC nor express HTLV-1 proteins. The HTLV-1–positive cells were only infiltrating CD4-positive T cells. These results suggest that HTLV-1–infected CD4-positive T cells, but not oligodendrocytes, are the main targets of HTLV-1–specific CTLs in the CNS, and that an interaction between these infected CD4-positive cells and CTLs may cause bystander damage in oligodendrocytes that is associated with demyelination. Similarly, in a previous study on an animal model of neurotropic mouse coronavirus infection, activated CD8-positive T cells specific to neither the virus nor CNS antigens caused demyelination (27). Mechanisms of demyelination in other viral infections in the CNS, even those exhibiting dense infiltration of activated CTLs such as measles or lymphocytic choriomeningitis virus encephalitis, are unclear. Whereas a CD8-positive CTL has been considered to be beneficial for the host infected by a certain virus by diminishing virus-infected cells, recent studies clearly show that strong CTL responses to a pathogen sometimes induce an immunopathology that is harmful to the host. For example, in a mouse model of CNS lymphocytic choriomeningitis virus infection, the depletion of CD8-positive T cells rescues the animal from a fatal condition (28). In another report, highly activated CD8-positive T cells in the brain were correlated with early CNS dysfunction in simian immunodeficiency virus infection (29). Similarly, markedly increased HTLV-1–specific CTLs in the CNS may induce the development of HAM/TSP.

Previous studies reported that the HTLV-1 antigen is hardly detected in PBMCs (30, 31), despite a high proviral

FIGURE 3. Frequency of human T-lymphotropic virus type-1 (HTLV-1)-1 Tax–specific cytotoxic T lymphocytes (CTLs) in CD8-positive lymphocytes. Double staining with anti-CD8 monoclonal antibody (mAb) (red) and HLA-A*0201/Tax11-19 or HLA-A*2402/Tax301-309 tetramer (green) was performed with confocal laser scanning microscopy (CLSM). DAPI (blue) was used for counterstaining the nuclei. The 3 colors were captured sequentially using CLSM. Merged images are shown in the right-hand column. **(A–C)** Spinal cords from the 3 patients with HAM/TSP were stained with the tetramers. CTLs stained with the tetramer were exclusively positive for CD8. The arrowheads indicate CTLs. **(A)** Double staining with HLA-A*0201/Tax11-19 tetramer and anti-CD8 mAb (Patient 8624). HTLV-1–specific CTLs are observed in the parenchyma and comprise 29% of CD8-positive cells in the field. **(B)** Double staining with HLA-A*2402/Tax301-309 tetramer and anti-CD8 mAb (Patient 6315). The CTLs comprise 25% of CD8-positive cells in the field. **(C)** Double staining with HLA-A*2402/Tax301-309 tetramer and anti-CD8 mAb (Patient 6664). CTLs are visible in the perivascular area and comprise 11% (1 of 9) of CD8-positive cells in the field. **(D)** Double staining with HLA-A*2402/HIV Gag tetramer (tetramer control) and CD8 in Patient 6315. No cells are stained with the tetramer. **(E)** To corroborate the staining with the tetramer, an HLA pentamer was used for double staining (Patient 8624). Similarly, fluorescence of the HLA-A*02/Tax11-19 pentamer (red in left-hand column) is exclusively colocalized with that of CD8 (green in middle column), as shown by yellow in the merged image (right-hand column) in the thickened meninges. The percentage of Tax pentamer–positive cells in CD8-positive cells is 31% (5 of 16) of the CD8-positive cells in the field. White bars indicate 20 μm.

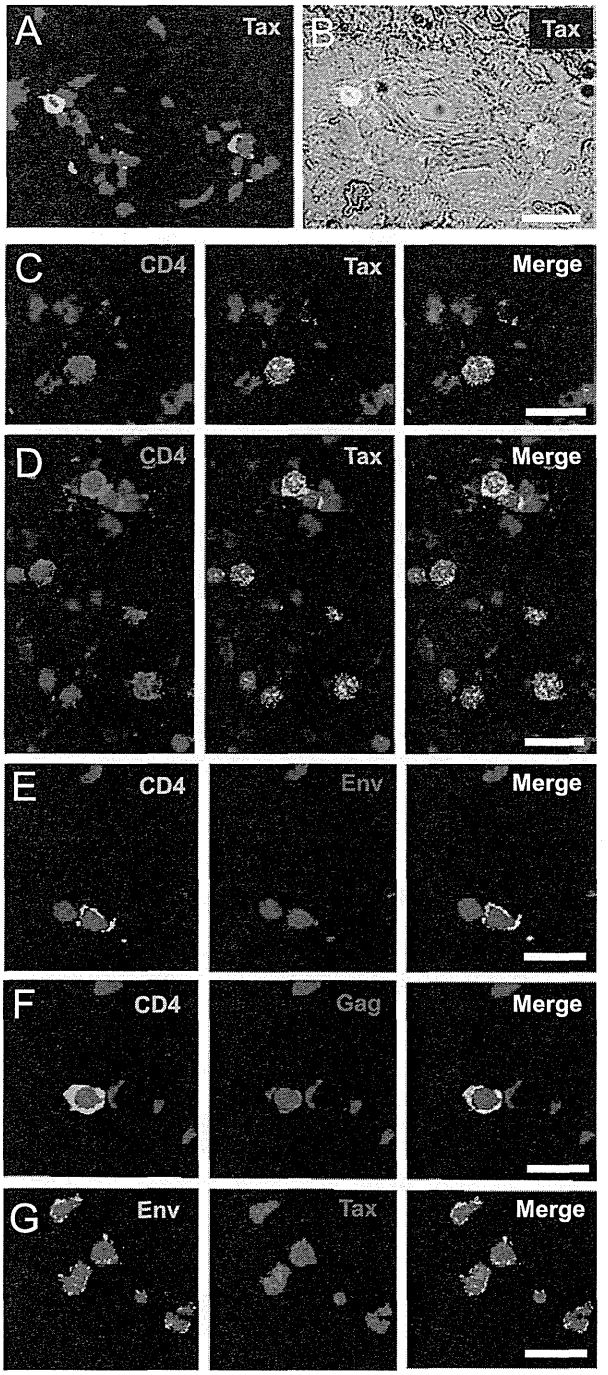

FIGURE 4. Detection of CD4-positive human T-lymphotropic virus type-1 (HTLV-1)–infected cells in CNS parenchyma. **(A, B)** Cells expressing HTLV-1 Tax protein were found near the vessels of the spinal cord of Patient 6315. **(C, D)** Double staining for CD4 (purple) and HTLV-1 Tax (green) revealed that visualized HTLV-1 Tax showed a patchy staining pattern in the nuclei in parenchyma **(C)** and in meninges **(D)**. **(E)** Double staining for CD4 (green) and HTLV-1 Env protein (red) revealed that HTLV-1 Env is costained with CD4 on the cell surface. **(F)** Double staining for CD4 (green) and HTLV-1 Gag protein (red) revealed that HTLV-1 Gag is detected in the cytoplasm of CD4-positive cells. **(G)** Double staining for HTLV-1 Env (green) and HTLV-1 Tax (red) revealed that both proteins were detected separately in the same cells. The nuclei were counterstained with DAPI. White bars indicate 20 μm.

load (12). We also failed to detect any HTLV-1 proteins by the immunohistochemical or flow cytometric study in PBMCs from 20 HAM/TSP patients, even though the proteins became detectable after short-term culturing (Figure, Supplemental Digital Content 1, part C, http://links.lww.com/NEN/A676). Although the evidence of both vigorous persistent CTLs immune responses and increased IgM antibody specific for HTLV-1 in the peripheral blood of HAM/TSP patients have suggested that

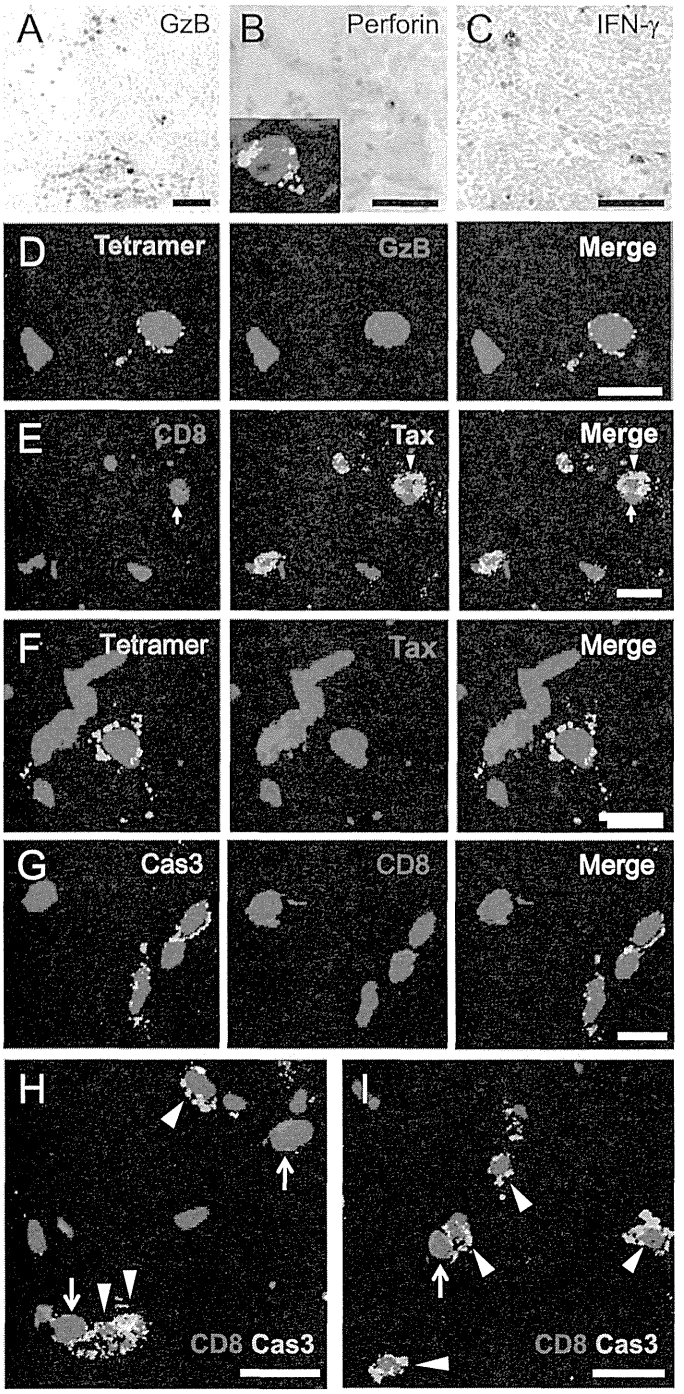

FIGURE 5. Cytotoxic T-lymphocyte (CTL) molecules in the CNS. **(A–C)** Immunohistochemistry shows granzyme B (GzB)–positive cells **(A)**, perforin-positive cells **(B)**, and interferon-γ (IFN-γ)–positive cells **(C)** in the perivascular area of the spinal cord of Patient 8624. Black bars indicate 100 μm. **(D)** Double staining with HLA-A*2402/Tax301-309-tetramer (green) and anti–granzyme B monoclonal antibody (mAb) (red) reveals a GzB-positive HTLV-1–specific CTL in the parenchyma of the spinal cord (Patient 6315). **(E)** A cell expressing HTLV-1 Tax protein is in contact with a CD8-positive cell in the spinal cord of Patient 6315. **(F)** An HTLV-1 Tax–specific CTL is next to the cell expressing Tax protein in the spinal cord of Patient 8614. **(G–I)** Double staining for active caspase-3 (Cas3) (green) and CD8 (red, arrows in **[H]** and **[I]**) reveals CD8-positive cells in contact with active caspase-3–positive cells in the spinal cord of Patient 8624. Nuclei were counterstained with DAPI. White bars indicate 10 μm.